Stony Brook University

Physiological and Pathological Roles of Class IA Phosphoinositide 3-Kinases p110α and p110β

A Dissertation Presented

by

Chia-yen Wu

to

The Graduate School

in Partial Fulfillment of the

Requirements

for the Degree of

Doctor of Philosophy

in

Molecular and Cellular Biology

(Biochemistry and Molecular Biology)

Stony Brook University

May 2010

Stony Brook University

The Graduate School

Chia-yen Wu

We, the dissertation committee for the above candidate for the
Doctor of Philosophy degree, hereby recommend
acceptance of this dissertation.

Richard Z. Lin, M.D.
Professor, Department of Medicine & Physiology and Biophysics

James Konopka, Ph.D.
Professor, Department of Molecular Genetics and Microbiology

Ira S. Cohen, Ph.D.
Leading Professor, Department of Physiology and Biophysics

Hsien-yu Wang, Ph.D.
Associate Professor, Department of Physiology and Biophysics

Howard Crawford, Ph.D.
Associate Professor, Department of Pharmacological Sciences

This dissertation is accepted by the Graduate School

Lawrence Martin
Dean of the Graduate School

Abstract of the Dissertation

Physiological and Pathological Roles of Class IA Phosphoinositide 3-Kinases p110α and p110β

by

Chia-yen Wu

Doctor of Philosophy

in

Molecular and Cellular Biology

(Biochemistry and Molecular Biology)

Stony Brook University

2010

Class I phosphatidylinositol 3-kinases (PI3Ks) are enzymes that phosphorylate the 3'-OH of the inositol moiety of the membrane lipid phosphatidylinositol 4,5-bisphosphate. These enzymes are divided into subclasses IA and IB. Class IA PI3Ks play essential roles in regulating cell growth, survival and metabolism. They are also strongly implicated in the development of human cancers. There are three class IA PI3K catalytic isoforms, p110α, p110β and p110δ. Currently, it is unclear what are their distinct biological functions. For my thesis research, I used genetically engineered

mice to study the roles of p110α and p110β in the regulation of heart contraction, the maintainence of skeletal muscle mass and the development of pancreatic cancer. Ablation of p110α or p110β alone in cardiac myocytes resulted in a relatively mild or minimal phenotype, respectively. However, mice lacking both p110α and p110β died less than 40 days after birth with 100% penetrance. The Ca^{2+}-handling system that is essential for excitation-contraction coupling was severely disrupted in the double PI3K-null myocytes. The second component of my thesis research investigated PI3Ks in the skeletal muscle. Mice lacking p110α had smaller skeletal muscle mass than wild type animals, whereas loss of p110β did not affect muscle mass. By contrast, mice lacking PTEN, a phosphatase that antagonizes PI3K signaling, had increased skeletal muscle mass. Insulin-like growth factor-1 activation of PI3K signaling was blocked in the p110α-null, but not p110β-null, muscles. The final component of my thesis research investigated the role of PI3Ks in oncogenic Kras-induced pancreatic tumors. Kras mutations are found in > 90% of human pancreatic ductal adenocarcinomas (PDA). Oncogenic Kras-induced PDA in a mouse model was completely blocked by genetic deletion of p110α but not affected by the loss of p110β. These studies indicate that PI3K p110α and p110β play distinct roles in regulating different physiological and pathological functions in a tissue-specific manner. These results may have clinical implications for the use of PI3K inhibitors in the treatment of diseases such as cancer.

Table of Contents

Chapter 2
Essential Roles of p110α and p110β in Maintaining Cardiac Contraction

Chapter 3
Differential Regulation of Skeletal Muscle Mass by p110α and p110β

Chapter 4
Differential Roles of p110α and p110β in Kras-Induced Pancreatic Tumorigenesis

List of Figures

Chapter 1

Chapter 2

Chapter 3

Chapter 4

List of Tables

Chapter 1

Chapter 2

List of Abbreviations

4E-BP1	4E-binding protein 1
AMPK	AMP-activated protein kinase
aPKC	atypical protein kinase C
BSA	bovine serum albumin
C2 domain	protein kinase C homology-2
CSQ2	calsequestrin-2
EGF	epidermal growth factor
EGFR	epidermal growth factor receptor
FBS	fetal bovine serum
FOXO	Forkhead box O
GAP	GTPase-activating protein
GEF	GTP/GDP-exchange factor
GPCR	G protein-coupled receptors
GSK3	glycogen synthase kinase 3
HER2	human epidermal growth factor receptor 2
Het	heterozygous
Hom	homozygous
$I_{Ca,L}$	L-type Ca^{2+} currents
IGF-1	insulin-like growth factor 1
IGFR	insulin-like growth factor receptor
IR	insulin receptor
IRS-1	insulin receptor substrate 1

IVC	inferior vena cava
JP-2	junctophilin-2
jSR	terminal cisterna of the sarcoplasmic reticulum
KD	kinase-dead
KRas*	oncogenic Kras^{G12D} mutant/LSL-Kras^{G12D};Ptf1a-Cre
LTCC	L-type Ca^{2+} channel
MAFbx	muscle atrophy F-box
MCK	muscle creatine kinase
MEF	mouse embryonic fibroblast
MHC	myosin heavy chain
mTOR	mammalian target of rapamycin
mTORC1	mTOR/raptor complex
mTORC2	mTOR/rictor complex
MuRF-1	muscle ring finger-1
PanIN	pancreatic intraepithelial neoplasia
PBD	p21-binding domain
PDA	pancreatic ductal adenocarcinoma
PH domain	pleckstrin homology domain
PI	phosphatidylinositol
PI3K	phosphoinositide 3-kinases
PDGF	platelet-derived growth factor
PDK1	phosphoinositide-dependent kinase 1
PNPP	p-nitrophenyl phosphate
PRAS40	proline-rich Akt substrate

PTEN	phosphatase and tensin homologue deleted on chromosome ten
RBD	Ras-binding domain
RyR	ryanodine receptor 2
S6K1	ribosomal protein S6 kinase 1
SERCA2	SR Ca^{2+}-ATPase-2
SH2 domain	src homology region
SR	sarcoplasmic reticulum
TSC2	tuberous sclerosis 2
T-tubule	transverse tubule

Acknowledgements

For me to be able to accomplish my thesis research, first I would like to thank my advisor, Dr. Richard Z. Lin, who gave me a great opportunity to work on interesting and significant research projects. I have learned and accumulated lots of experience and knowledge. Dr. Lin was always very patient and considerate in person; full of excellent ideas and logical thoughts in his mind. With all these, he has helped me and taught me so much that I could finish my PhD life happily. I really appreciate that I was so lucky to have such a wonderful advisor.

In addition, I would like to thank my committee members, who looked at my progress on research so carefully to keep me on the right direction and not being lost. Everyone gave me helpful suggestions and new thoughts from different angles which expanded my research views.

Also, I would like to thank my friends, both in Taiwan and in the U.S., together with my lab members, who support me and encourage me when I was upset and stressful. They always cheered me up at the right timing to make me feel energetic and refreshed again.

Most importantly, I would like to thank my family and my fiancé, who are always there for me. Their confidence on me, their encouragement and support, and their words for me are all irreplaceable. Without them, I could never finish my study and get my PhD degree!

Chapter 1

Introduction to Phosphoinositide 3-Kinases

1-1 General Introduction

1-1-1 Phosphatidylinositol

Phosphatidylinositol (abbreviated PI) is a negatively charged phospholipid and a component of the cytosolic side of eukaryotic cell membranes (Fig. 1-1). In cells, the free –OH groups at the 3', 4', or 5' positions of the inositol ring can be phosphorylated in different combinations by a variety of kinases to generate seven phosphoinositides: PI(3)P, PI(4)P, PI(5)P, $PI(4,5)P_2$, $PI(3,5)P_2$, $PI(3,4)P_2$ and $PI(3,4,5)P_3$.

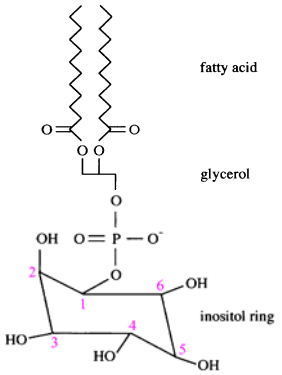

Fig. 1-1 Phosphatidylinositol

1-1-2 The Discovery of Phosphoinositide 3-Kinases

Phosphoinositide 3-kinases (PI3Ks) are lipid kinases which phosphorylate PI or phosphoinositides at the 3' position of the inositol ring[1-2]. It has been two decades since PI3Ks were discovered[3]. This family of proteins was first observed in studies of oncogenic and mitogenic signal transduction where increased levels of 3-phosphorylated PIs such as PI(3)P and $PI(3,4,5)P_3$ were found in transformed and/or mitogen-stimulated cells[4-5]. These enzymes were shown to physically interact with tyrosine-phosphorylated proteins such as the polyomavirus middle T antigen–$pp60^{c\text{-}src}$ complex[6] and the platelet-derived growth factor (PDGF) receptor[4] and were activated by insulin[7]. One

component of the PI3K complex, the p85 subunit, was purified using affinity probes and then cloned[8-10] in the early 1990s. The p85 subunits are regulatory subunits containing one SH3 domain and two SH2 domains (src homology regions) that mediate the interaction of PI3K with tyrosine-phosphorylated proteins. Subsequently, the first PI3K p110 catalytic subunit was identified and cloned. It forms a tight association with the p85 subunit[11-12] and was shown to contain the catalytic activity of the prototypic p110/p85 PI3K heterodimer. After that, many other PI3K catalytic isoforms were identified using biochemical approaches and cloning strategies from diverse eukaryotes, including yeast, flies, mammals and plants.

1-2 The PI3K Family

Based on their protein domain structure, associated regulatory subunits, and *in vivo* lipid substrate specificity, PI3Ks can be divided into three groups: Class I, Class II, and Class III[1, 3, 13]. All the PI3K catalytic subunits share a homologous region that consists of a catalytic domain linked to a C2 (protein kinase C homology-2) domain and a helical domain.

1-2-1 Class I PI3Ks

The preferred *in vivo* substrate for Class I PI3Ks is $PI(4,5)P_2$ to produce $PI(3,4,5)P_3$, an essential intracellular second messenger[2]. Based on the ability to bind different regulatory subunits, Class I PI3Ks are further grouped into subclasses IA and IB. Class IA p110α, p110β and p110δ catalytic subunits associate with p85 regulatory subunits (50-85 kDa) and the Class IB p110γ catalytic subunit interacts with a p101 or p84 regulatory

subunit.

Class IA PI3Ks play an essential role in regulating physiological cellular events including growth, survival and metabolism[14-15]. Furthermore, dysregulation of Class IA PI3K signaling is strongly implicated in the development of human cancers[16-17]. However, the distinct biological functions of the three Class IA catalytic isoforms had been unclear until recently, when studies using whole-body p110 knockout mouse models began to address this research question. Mice with germline deletion of the broadly expressed isoform p110α (encoded by *Pik3ca*) or p110β (encoded by *Pik3cb*) die as embryos[18], whereas mice with deletion of p110δ, found mainly in leukocytes, have a range of immunological defects[18]. A number of other research strategies have been used to address the isoform-specific functions of these PI3Ks, including tissue-specific PI3K isoform knockout mice, whole-body PI3K mutant "knockin" mice or use of isoform-specific pharmacological inhibitors. Results of some of these studies are summarized in Table 1.

Table 1 Genetically modified animal models of p110α and p110β.

	MEFs	Mouse Physiology	Mouse Pathology
p110 α	$\alpha^{-/-}$ blocks transformation by oncogenic Hras, HER2, EGFR[2, 4]	α KD knockin (het) retards animal growth[3]	α knockin mutant (can't bind Ras) blocks Kras-driven lung tumorigenesis[1]
	α knockin mutant (can't bind Ras) blocks transformation by oncogenic Hras and EGFR[1]	$\alpha^{-/-}$ heart is smaller and has reduced contractility[6]	
p110 β	$\beta^{-/-}$ blocks transformation by oncogenic Hras and EGFR[4]	β KD knockin (hom) mice have retarded growth[5]	$\beta^{-/-}$ blocks prostate tumorigenesis driven by PTEN loss[4]
			β KD knockin (hom) blocks HER2-driven mammary gland tumorigensis[5]

1) Gupta *et al. Cell* (2007); 2) Zhao *et al. PNAS* (2006); 3) Foukas *et al. Nature* (2006);
4) Jia *et al. Nature* (2008); 5) Ciraolo *et al. Science Signaling* (2008); 6) Lu *et al. Circulation* (2009)

MEF: mouse embryonic fibroblast; KD: kinase-dead; Het: heterozygous; Hom: homozygous; HER2: human epidermal growth factor receptor 2; EGFR: epidermal growth factor receptor.

Class IB p110γ also shows a restricted tissue distribution—it is abundant in cells of haematopoietic origin and is present at low concentrations in endothelia, smooth muscle cells and cardiomyocytes[14]. Mice with whole-body genetic deletion of p110γ are viable[19]. This PI3K is involved in inflammatory processes[20-21] and cardiovascular function[22].

1-2-2 Class II PI3Ks

Class II PI3Ks are large molecules (>170 kDa) whose C2 domains are located at the C terminus of the proteins[3]. There are three class II enzymes—PI3K-C2α, PI3K-C2β and PI3K-C2γ—encoded by three distinct genes. They are thought to act as monomeric enzymes[23]. The main *in vivo* substrate of class II PI3Ks has remained elusive for a long time, but more and more evidence suggests that it might be PI. Recently, one study reported that in the insulin signaling cascade, PI(3)P is the sole *in vivo* product of C2α[24]. Also, by using RNAi, it has been shown that C2α has an important role in controlling cell survival[25] and cell growth[26].

1-2-3 Class III PI3Ks

The only known class III enzyme is the homologue of the *Saccharomyces cerevisiae* membrane trafficking protein Vps34, which associates with a 150 kDa protein that is the homologue of Vps15[13, 27]. Class III PI3K utilizes only PI as a substrate. Class III PI3K is required for the induction of autophagy during nutrient deprivation in yeast and in mammalian cells[28]. Recent studies also suggest that mammalian hVps34 is required for the activation of the mTOR (mammalian target of rapamycin)/S6K1 (ribosomal protein S6

kinase 1) pathway, which regulates protein synthesis in response to nutrient availability[29].

1-3 Class I PI3K Activation and Signaling

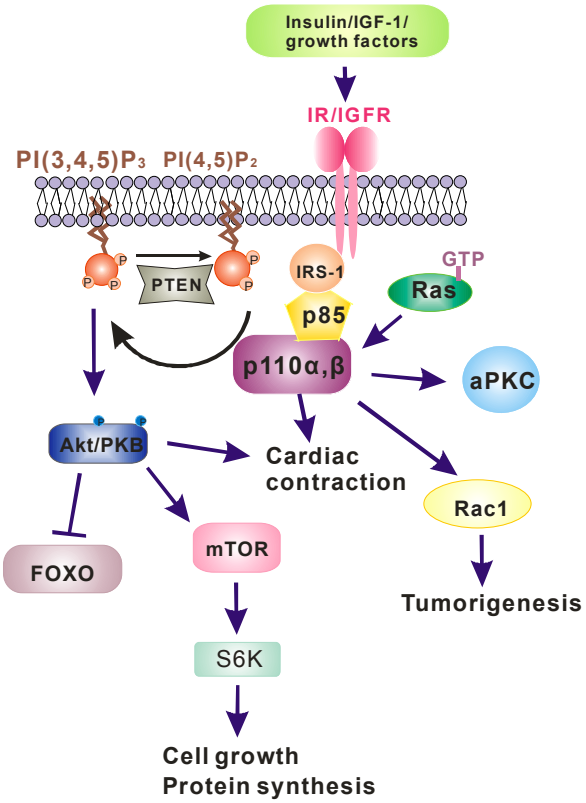

Fig. 1-2 A simplified PI3K signaling pathway. IGF-1: insulin-like growth factor 1; IR: insulin receptor; IGFR: insulin-like growth factor receptor; IRS-1: insulin receptor substrate 1; PTEN: phosphatase and tensin homologue deleted on chromosome ten; aPKC: atypical protein kinase C; mTOR: mammalian target of rapamycin; FOXO: Forkhead box O; S6K: ribosomal protein S6 kinase.

1-3-1 PI3K Activation

Class I PI3Ks are activated by a wide variety of different stimuli including growth factors, inflammatory mediators, hormones, neurotransmitters and immunoglobulins/antigens (Fig. 1-2)[1, 30]. The association of the catalytic subunits with the

regulatory subunits is critical for their activation. The SH2 domains of Class IA p85 regulatory subunits bind with high affinity to phosphorylated tyrosine motifs present in growth factor receptors such as the insulin receptor (IR) or insulin-like growth factor 1 (IGF-1) receptor, their substrates, or receptor-associated adaptor proteins such as insulin receptor substrate 1 (IRS-1)[31]. In addition, p110β can be activated by G protein-coupled receptors (GPCRs) without the binding of p85 to tyrosine-phosphorylated proteins[32]. Instead, the mechanism of activation is through binding of the p110β subunit to βγ-subunits of heterotrimeric GTP-binding proteins. Similarly, Class IB p110γ is activated by Gβγ[14]. All four Class I PI3K catalytic subunits can also be activated directly by the small GTPase Ras (Fig. 1-2)[33] and the ability of Ras or Ras family members to activate PI3Ks has been shown to depend on the isoform of PI3K involved[34].

1-3-2 Signaling by PI3Ks

1-3-2-1 PTEN

PTEN (phosphatase and tensin homologue deleted on chromosome ten; Fig. 1-2) was identified as a tumor suppressor and found to be frequently mutated in sporadic glioblastomas and in cancers of the prostate and breast[35-36]. PTEN is a phosphatase specific for the 3'-position of the inositol ring of phosphoinositides[37] (Fig. 1-2). It was shown in many cell types that PTEN decreases cellular $PI(3,4,5)P_3$ levels[38-39]. In addition, identification of PTEN as a functional antagonist of PI3Ks was supported by genetic evidence in different systems such as *C. elegans* and *D. melanogaster*[13]. The loss or mutation of PTEN in various cancers leads to hyperactive signaling downstream of PI3K[40]. Loss of PTEN function is now considered one of the most common genetic

alterations in human cancers[41].

1-3-2-2 Akt/PKB

The second messenger $PI(3,4,5)P_3$ binds to adaptor and effector proteins containing pleckstrin homology (PH) domains and drives several downstream signaling cascades. The best known PI3K effector is the protein kinase Akt/PKB[1] (Fig. 1-2). This kinase is the cellular homologue of the viral oncoprotein v-*Akt,* hence the name Akt[14].The alternative name PKB comes from its homology to PKA and PKC. There are three isoforms of Akt/PKB: Akt1/PKBα, Akt2/PKBβ, and Akt3/PKBγ. The N-terminal PH domain of Akt/PKB (called Akt hereafter) binds to $PI(3,4)P_2$ and $PI(3,4,5)P_3$ that are produced following PI3K activation, causing Akt to translocate to the membrane. Two specific sites, T308 in the kinase domain and S473 (in Akt1) in the C-terminal tail, need to be phosphorylated for full activation of Akt. T308 is phosphorylated by phosphoinositide-dependent kinase 1 (PDK1). S473 is phosphorylated by the mTOR/rictor complex (mTORC2)[42]. Once activated, Akt phosphorylates a plethora of downstream proteins, such as Forkhead box O (FOXO) transcription factors[43] and glycogen synthase kinase 3 (GSK3)[44-45], that regulate many different cellular processes including cell survival, apoptosis and metabolism.

1-3-2-3 mTOR

The protein kinase mTOR (Fig. 1-2) is both a downstream effector and upstream regulator of Akt. It is now known that mTOR exists in two distinct multi-protein complexes: a rapamycin- and nutrient-sensitive complex mTORC1 and a rapamycin- and nutrient-insensitive complex mTORC2[46]. Akt activates mTORC1 by phosphorylating both

the 40 kDa proline-rich Akt substrate (PRAS40) and tuberous sclerosis 2 (TSC2; also known as tuberin) proteins to attenuate their inhibitory effects on mTORC1. The most extensively studied mTORC1 downstream effectors are S6K (Fig. 1-2) and eukaryotic translation initiation factor 4E-binding protein 1 (4E-BP1)[47], which play an important role regulating protein synthesis and cell growth. On the other hand, the mTORC2 complex directly regulates Akt by phosphorylating the S473 site[46, 48].

1-3-2-4 GTPases

Cycling between inactive and active forms of small GTPases is regulated by GTP/GDP-exchange factors (GEFs)[49] and GTPase-activating proteins (GAPs)[50]. GEFs activate small GTPases by catalyzing the release of GDP and binding to GTP, whereas GAPs stimulate GTP hydrolysis to convert the proteins from the active form back to the inactive GDP-bound state. PH domains were found in all GEFs specific for the Rho family of GTPases and these GEFs show specificity for binding $PI(3,4,5)P_3$; therefore, Class I PI3K activity has been implicated in the activation of Rho family GTPases, including Rac (Fig. 1-2). Increases in GTP-loaded Rac in response to PDGF have been shown to be mediated by PI3K[51]. ARAP3, a GAP of Rho, triggers cellular cytoskeletal changes in response to PI3K activity[52]. It is believed that PI3K regulation of the actin cytoskeleton structure through Rac/Rho GTPases plays a role in cancer cell migration and metastasis[1].

1-4 The Role of Class I PI3Ks in Cellular Functions and Diseases

1-4-1 Cell Growth

In post-mitotic cells such as cardiac myocytes, PI3K signaling controls growth. For example, overexpression of constitutively active PI3K p110α in the heart results in increased cell and heart size, while dominant-negative p110α results in smaller hearts and cardiac myocytes[53]. Expression of activated Akt also increases heart size[54]. Similarly, deletion of PTEN in a tissue-specific manner leads to increased organ and cell sizes[55]. PI3K signaling also controls the overall body size in mammals and other organisms. Mice heterozygous for an inactive p110α mutant exhibit retarded growth[18]. Similar growth retardation is observed in mice expressing a kinase-dead mutant of p110β[56]. Akt1 knockout mice are smaller compared to the littermate controls[57]. Mice with deletion of both Akt1 and Akt2 are much smaller and die at a young age[58]. mTOR is the central controller of cell growth. Activation of Akt by PI3K leads to TSC2 phosphorylation, activation of mTOR and phosphorylation of its downstream effectors S6K and 4E-BP1, and increased protein synthesis and cell growth[59]. Conditional deletion of raptor (one of the proteins in mTORC1)[60] or S6K1[61] also results in smaller organ size and reduced growth[62].

1-4-2 Cardiac Contraction

Contraction of cardiac myocytes is initiated by an inward Ca^{2+} current ($I_{Ca,L}$) through the voltage-dependent L-type Ca^{2+} channel (LTCC), followed by a much larger release of Ca^{2+} from the sarcoplasmic reticulum (SR). p110γ-null mice exhibit increased cardiac contractility[22] that is due to the localized production of cAMP that increases SR Ca^{2+}

content and release but not $I_{Ca,L}$[63]. By contrast, expression of dominant-negative p110α in the heart does not cause a change in cardiac contractility or $I_{Ca,L}$ density[22, 64]. These results led to the belief that Class IA PI3Ks regulate heart size whereas Class IB PI3K controls heart contraction. A recent study from our laboratory shows that inducible ablation of p110α, but not p110β, in cardiac myocytes of adult mice results in reduced $I_{Ca,L}$ and compromised cardiac contractile function[65]. Thus, p110α promotes and p110γ reduces cardiac contractility. Reduced PI3K/Akt signaling in the heart of diabetic mice also causes a contractile defect and reduced $I_{Ca,L}$[66].

1-4-3 Cell Proliferation and Survival

PI3K controls cell growth, proliferation, and survival, which constitute critical steps towards tumor formation and malignant cell dissemination. Genetic alterations in the PI3K pathway have been associated with cancers[36]. The most frequent of these alterations found in various human cancers are loss of PTEN[40] and mutations in p110α[67], both leading to elevated production of $PI(3,4,5)P_3$. Table 2[68] summarizes the changes in PI3K/Akt signaling molecules that lead to tumor formation.

Table 2 Genetic alterations in the PI3K/Akt pathway in cancer.

Pathway Component	Type of Alteration	Tumor Lineage
PTEN	Loss-of-function by somatic mutation	Brain, prostate, endometrium
	Germline mutation (in 80% of Cowden Disease)	Cowden disease: Increased risk for breast, thyroid, genitourinary and endometrial cancer
	Transcriptional down-regulation (e.g., promoter methylation)	Melanoma, breast, colon
	Loss of heterozygosity	Prostate, melanoma, thyroid, breast, pancreas, ovary, brain, bladder, endometrium, cervix, head and neck, kidney, lung
p110α	Gain-of-function by somatic mutation	Colon, breast, brain, ovary
	Amplification	Ovary, gastric, lung, cervix
p85	Gain-of-function by somatic mutation	Brain, colon, ovary
AKT1	Gain-of-function by somatic mutation	Breast, colorectal, ovary
AKT2	Amplification	Ovary, lymphoma, pancreas
	Mutation	Colorectal
PDK1	Mutation	Colorectal
TSC 1/2	Loss-of-function by mutation (occasionally with concomitant loss of heterozygosity for the wild type allele)	Tuberous sclerosis (hamartomas of the skin, brain and kidney; rare progression to malignancy)

Arcaro, A. & Guerreiro, A.S. *Curr Genomics* **8**, 271-306 (2007)

Akt can promote the G1-S phase transition by phosphorylating FOXO transcription factors, causing them to exit the nucleus and thus blocking the transcription of cell cycle inhibitors such as p27Kip1[31]. In addition, Akt phosphorylation of GSK3 causes an increase in expression of cyclin D1[31]. Two anti-apoptotic proteins, Bcl-2 and Bcl-X_L, are released from the pro-apoptotic protein Bad after being phosphorylated by Akt, thus promoting cell survival. Another way that Akt can promote cell survival is by blocking FOXO-mediated transcription of pro-apoptotic genes[69]. mTOR also plays a role in promoting cell cycle progression, as mTOR knockout embryos have severely impaired cell proliferation[70]. Mouse embryonic fibroblasts (MEFs) lacking p110β also have reduced cell proliferation that might be due in part to defective activation of mTOR signaling[71].

1-4-4 Glucose Metabolism

PI3K activation is considered to play a critical role in insulin-induced glucose metabolism in muscle, adipose tissue, and liver. Impaired PI3K/Akt signaling is associated with glucose intolerance and insulin resistance, which play a major role in the occurrence and development of Type 2 diabetes mellitus[72]. Mice heterozygous for an inactive mutant of PI3K p110α have increased adipose tissue and show impaired glucose tolerance and insulin sensitivity[18]. Germline knockin of kinase-dead p110β results in mild insulin resistance in older animals[56]. These results are consistent with a number of studies showing that insulin signaling goes mainly through p110α[18, 73-74]. Deletion of Akt2 results in impaired ability of insulin to lower blood glucose and altered glucose homeostasis[75]. Ablation of S6K1 causes hypoinsulinemia and mild glucose intolerance but protects from age- and diet-induced obesity due to enhanced insulin sensitivity[76-77].

1-4-5 Cell Motility and Migration

As mentioned earlier, the Rho family members Rho, Rac, and cdc42 have been extensively studied for their ability to regulate cytoskeketal dynamics at different stages of cell migration. Evidence suggests that PI3Ks are involved in and crosstalk with Rho family pathways at these cell migration stages: polarization, protrusion, and adhesion[78]. Germline or endothelial cell-specific inactivation of p110α led to severe defects in vascular remodeling because p110α normally regulates cell migration through RhoA[79]. In response to epidermal growth factor (EGF), Ras is required for both $PI(3,4,5)P_3$ production and protrusion, whereas Rac1 is required to stabilize adhesive structures for cell mobility[80].

1-5 Aim of the Dissertation

To study the roles of p110α and p110β, we generated conditional knockout mice for these genes (p110α$^{Flox/Flox}$ and p110β$^{Flox/Flox}$ mice)[65]. These animals were bred to mice expressing Cre recombinase under the control of a tissue-specific promoter, leading to the tissue-specific ablation of p110α or p110β. In this dissertation thesis, I will present my findings on the physiological and pathological functions of p110α and p110β in three different systems: regulation of cardiac contraction (Chapter 2), skeletal muscle mass (Chapter 3), and pancreatic tumorigenesis (Chapter 4).

Chapter 2

Essential Roles of p110α and p110β in Maintaining Cardiac Contraction

2-1 Introduction

Efficiency of cardiac mechanical function depends on intricate contractile structures and tightly regulated Ca^{2+} fluxes. In mammalian myocardium, the Ca^{2+}-handling proteins are concentrated at the cardiac dyad that consists of an invagination of the plasma membrane called the transverse tubule (T-tubule)[81-82] juxtaposed to a single terminal cisterna of the sarcoplasmic reticulum (jSR)[83]. The periodicity of T-tubules and their juxtaposition to the sarcoplasmic reticulum (SR) is necessary for efficient Ca^{2+} release in myocytes. The voltage dependent L-type Ca^{2+} channels (LTCCs) that initiate myocyte contraction are concentrated at the T-tubules. Across from the T-tubules, the jSR membrane, within nanometer distance, contains the ryanodine receptor 2 (RyR) and its binding partners triadin[84] and junctin[85]. The RyR is activated by the relatively small Ca^{2+} current that enters through the LTCC to release a much larger amount of Ca^{2+} from the SR, leading to myocyte contraction. The Ca^{2+} is then pumped back into the SR by the SR Ca^{2+}-ATPase-2 (SERCA2). The jSR lumen contains a high concentration of calsequestrin-2 (CSQ2) that binds Ca^{2+} and serves as a Ca^{2+} sink[86]. Junctophilin-2 (JP-2) is also found at this location and plays an important role in coordinating the colocalization of T-tubules with the jSR[87]. These molecules form the cardiac Ca^{2+} release units that are critical for proper excitation-contraction coupling in cardiac myocytes[88]. T-tubule formation and establishment of mature cardiac dyads occur after birth in mice. Currently,

little or no information is available regarding the regulation of expression of Ca^{2+}-handling proteins found in the cardiac dyad.

Cardiac myocytes express p110α, p110β and p110γ. Cardiac contractility was shown to increase in p110γ-null mice as a result of increased cAMP levels[22]. Because whole-body ablation of p110α or p110β results in embryonic lethality[89-90], in earlier work we used Cre-lox mouse models to study the effects of ablating either p110α or p110β in the heart[65]. The loss of p110α, but not p110β, resulted in a mild contractile defect due to decreased current through the LTCC. However, little is known about cardiac consequences of downregulating multiple PI3Ks concurrently. In this study, we investigated the effect of ablating both p110α and p110β in the heart.

2-2 Materials and Methods

General Materials

Antibodies were purchased from commercial sources: p110α and p110β from Cell Signaling Technology; pan-p85 from Millipore; $Ca_V1.2$ from Alomone Labs; RyR, SERCA2 and CSQ2 from Affinity Bioreagents; triadin from Santa Cruz Biotechnology; JP-2 from Sigma Aldrich; and caveolin-3 from BD Transduction Laboratories. Di-8-ANEPPS, goat anti-rabbit antibody conjugated to Alexa Fluor 488 and goat anti-mouse antibody conjugated to Alexa Fluor 647 were from Invitrogen.

Animals

All animal-related experimental protocols were approved by the Stony Brook University Institutional Animal Care and Use Committee. All genetically modified mice

were in a mixed C57BL/6 and 129 genetic background. We used a breeding program between $p110\alpha^{Flox/WT}$ and $p110\beta^{Flox/WT}$ mice[65] and transgenic mice carrying the Cre recombinase gene under the control of the muscle creatine kinase promoter (MCK-Cre). Offspring from the last breeding step have 16 possible genotypes: $p110\alpha^{Flox/Flox}$;$p110\beta^{Flox/Flox}$, $p110\alpha^{Flox/Flox}$;$p110\beta^{Flox//WT}$, $p110\alpha^{Flox/WT}$;$p110\beta^{Flox/Flox}$, $p110\alpha^{Flox/Flox}$;$p110\beta^{WT/WT}$, $p110\alpha^{WT/WT}$;$p110\beta^{Flox/Flox}$, $p110\alpha^{Flox/WT}$;$p110\beta^{WT/WT}$, $p110\alpha^{WT/WT}$;$p110\beta^{Flox/WT}$, and $p110\alpha^{WT/WT}$;$p110\beta^{WT/WT}$ that are plus or minus MCK-Cre. In this study, we used only $p110\alpha^{Flox/Flox}$;$p110\beta^{WT/WT}$;MCK-Cre, $p110\alpha^{WT/WT}$;$p110\beta^{Flox/Flox}$;MCK-Cre and $p110\alpha^{Flox/Flox}$;$p110\beta^{Flox/Flox}$;MCK-Cre mice, and those that did not express MCK-Cre served as controls. Phenotypic comparisons were made between knockout mouse strains and their p110-intact siblings.

Mouse Heart Membrane Preparation and Western Blotting

Mouse ventricular microsomes were prepared as previously described[91]. After immunoblotting, signals were visualized using an enhanced chemiluminescence kit (PerkinElmer Life Sciences), CSPD chemiluminescence kit (Applied Biosystems) or the Odyssey Infrared Imaging System (LI-COR Biosciences).

Electron Microscopy

Hearts were harvested, fixed immediately in 4.0% paraformaldehyde and 2.5% EM grade glutaraldehyde in 0.1 M PBS (pH 7.4), and chopped into small pieces in EM fixative. After fixation at 4°C overnight, samples were placed in 2.0% osmium tetroxide in 0.1 M PBS (pH 7.4), dehydrated in a graded series of ethyl alcohol, and embedded in Epon resin. Ultra-thin sections of 80 nm were cut with a Reichert-Jung UltracutE ultramicrotome, and placed on formvar coated slot copper grids. Sections were counterstained with uranyl acetate and lead citrate. Samples were viewed with a FEI Tecnai12 BioTwinG2 electron

microscope. Images were acquired with an AMT XR-60 CCD Digital Camera System.

Heart Histology

Hearts were fixed by perfusion with 10% buffered formalin and embedded in paraffin. Sections of 10 μm thickness were cut and stained with hematoxylin and eosin.

Di-8-ANEPPS Staining and Immunofluorescence Microscopy

The T-tubule network was visualized by incubating isolated ventricular myocytes with 10 μM di-8-ANEPPS for 10 min, followed by a 10 min washout period. Images were acquired using the Olympus FluoView^{TM} FV1000 imaging system. Di-8-ANEPPS was excited at 488 nm and emission intensity was measured at 506 nm. For spatial spectrum analysis, regions of interest without nuclei were first selected. In order to avoid staining variation and noise, average intensity was subtracted before any further computation. Power spectrum was computed by 1D fast Fourier transform along the longitudinal dimension for each sample, averaging multiple lines. Power ratios calculated as peak power divided by mean power from 0.2 to 0.4 μm^{-1} for each cell were averaged and used to compare groups of cells.

For colocalization experiments, isolated ventricular myocytes from control and dKO mice were fixed for 10 min in freshly made 3.7% formaldehyde solution, followed by 3 X 10 min washes in PBS. The cells were then permeabilized in a solution of PBS containing 0.2% Triton X-100 and 5% fetal bovine serum (FBS) for 5 min. The permeabilization solution was removed with 3 X 10 min washes in 1% FBS solution. After that, the cells were labeled simultaneously with rabbit anti-$Ca_v1.2$ and mouse anti-RyR primary antibodies diluted in 0.5% bovine serum albumin (BSA) solution overnight at 4°C. Next day, the cells were washed with 3 X 10 min washes in 1% FBS solution. The cells were then incubated in 0.5% BSA solution containing the appropriate secondary antibodies for 1 hr,

rinsed for 3 X 10 min with 1% FBS solution, and then mounted in VectaShield (with DAPI) (Vector Laboratories) for imaging using the Olympus FluoView^{TM} FV1000 imaging system. Colocalization analysis was done by commercial software purchased from Imaris (Bitplane Inc.). An unbiased automatic thresholding method[92] was applied before calculating Pearson's coefficients and colocalization percentages.

Sarcomere Length Measurement

Contractile properties of myocytes were assessed using a video-based myocyte sarcomere spacing acquisition system as previously described[65].

Ca^{2+} Transient Measurements

Myocytes were loaded with Fluo-4AM and Ca^{2+} transients measured with an IonOptix photometry system as previously described[65].

Electrophysiology

L-type Ca^{2+} currents ($I_{Ca,L}$) were recorded using the whole cell patch clamp technique described previously[65]. The values were normalized to individual cell capacitance (control, 149 ± 23 pF; $\alpha^{-/-}$, 93 ± 18 pF; $\beta^{-/-}$, 110 ± 7 pF; and dKO, 91 ± 13 pF) to calculate the $I_{Ca,L}$ density.

SR Ca^{2+} Content Measurements

Ventricular myocytes were allowed to adhere to laminin-coated plates (Invitrogen) at 37˚C for at least one hr. Then they were loaded with 2 μM Fura-2 AM (Invitrogen) for 45 min at room temperature and washed with Tyrode solution[65]. The cells were placed in a perfusion chamber and field-stimulated in Tyrode solution containing 1.8 mM Ca^{2+}. Cells were electrically stimulated at 1 Hz for 5 min. Immediately after the electrical stimulation was stopped, myocytes were exposed to 10 mM caffeine using a rapid perfusion system (SF-77B Perfusion Fast-Step, Warner Instrument). Excitation wavelengths of 360 and 380

nm were used to monitor the fluorescence signals of Fura-2. The area under the curve of the caffeine-stimulated peak was used as the estimate of total SR Ca^{2+} content. All experiments were conducted at room temperature.

Real-Time RT-PCR

RNA was isolated from hearts of 36-37 day-old mice using Tri reagent (Sigma Aldrich). RNA was converted to cDNA using the iScript cDNA synthesis Kit (Bio-Rad) and analyzed by real-time PCR using the SYBR Green PCR Kit (Qiagen) with a DNA Engine Opticon (MJ Research). Results were quantified using a previously described method[93]. Results were normalized to the expression of 18S RNA. Oligos used for real-time PCR are listed in the table below:

$Ca_V1.2$	ATCACCATGGAGGGCTGGAC
	TGTGGGCATGCTCATGTTTCG
RyR	GATTTGTGGACTATAACAGGGC
	TCCCCAGGGGCACAGATGTT
Triadin	CCTCTACCAGAGTTCTCT
	GGGAGGTTCTTCTATTTCT
SERCA2	AAGGAGAGATGGGGCTCCAACGA
	GGAACTTTGTCACCAACAGCAATTTC
Junctin	GAATGGGAGAAGAGGAGG
	GTCTCTACGGCCTTCTTC
JP-2	GGAGAGCACACCAGACT
	CGCCCCTTGGTCTCTAT
CSQ2	GAGCTTGTGGCCCAGGTC
	CGGTTTGTTAGGGATGAC
β-MHC	TGCAAAGGCTCCAGGTCTGAGGGC
	GCCAACACCAACCTGTCCAAGTTC
18S	CCTGCGGCTTAATTTGACTC
	CGGACATCTAAGGGCATCAC

Statistics

Numerical data are presented as mean ± S.E.M., mean ± 95% confidence interval or median ± 25 percentile as described in the figure legends. Comparison between groups

was evaluated using one-way ANOVA with *post-hoc* Fisher least significant difference test. Comparison between two groups was evaluated using Student's t-test or Wilcoxon rank-sum test. Results were considered significant if the P value was <0.05.

2-3 Results

2-3-1 Early Death of Cardiac PI3K Knockout Mice

We bred p110α$^{Flox/Flox}$ and p110β$^{Flox/Flox}$ mice to animals carrying a Cre recombinase transgene under the control of the muscle creatine kinase (MCK) promoter[94] to generate single knockout p110α$^{Flox/Flox}$;MCK-Cre and p110β$^{Flox/Flox}$;MCK-Cre mice ($\alpha^{-/-}$ and $\beta^{-/-}$, respectively) and double knockout p110α$^{Flox/Flox}$;p110β$^{Flox/Flox}$;MCK-Cre mice (dKO). Siblings that do not express Cre served as controls. As expected, the p110α and/or p110β proteins were appropriately ablated in the single and double knockout myocytes (Fig. 2-1a).

a

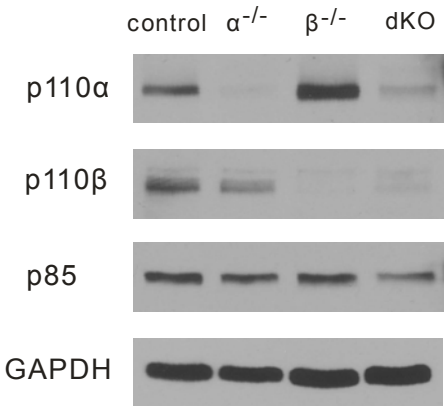

b

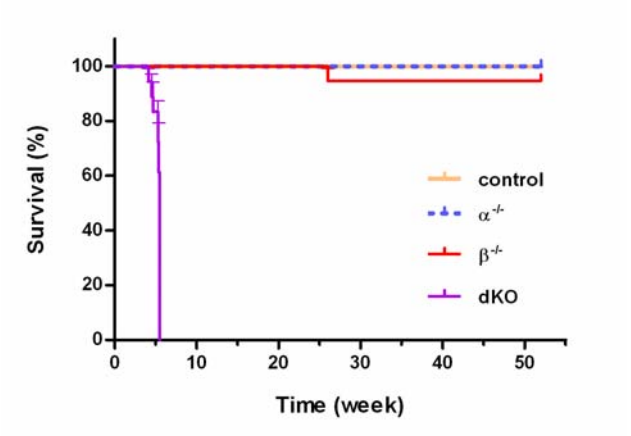

Fig. 2-1 Ablation of both p110α and p110β in cardiac myocytes causes early death in mice. (**a**) Lysates of myocytes isolated from the indicated groups of mice were analyzed by western blotting to detect the p110α and p110β PI3K catalytic subunits and the p85 regulatory subunit. GAPDH served as a loading control. (**b**) Kaplan Meier survival curves for control ($\alpha^{+/+}\beta^{+/+}$), p110$\alpha^{-/-}$ ($\alpha^{-/-}$), p110$\beta^{-/-}$ ($\beta^{-/-}$), and dKO ($\alpha^{-/-}\beta^{-/-}$) mice (N = 18 for dKO and N = 20 for the other 3 groups).

At birth, all four groups of mice behaved normally and were indistinguishable by outward appearance. However, all dKO mice died suddenly between 29-39 days of age (Fig. 2-1b). In contrast, there was no significant difference in the mortality rate of $\alpha^{-/-}$ or $\beta^{-/-}$ mice as compared to control animals for up to 1 year of age (Fig. 2-1b).

Examination of the dKO heart showed that both left and right ventricles were dilated, whereas no obvious gross changes were observed in the single PI3K knockout hearts (Fig. 2-2a). Higher magnification views of H&E-stained heart sections (Fig. 2-2b), as well as phase-contrast images of isolated myocytes (Fig. 2-4a), did not reveal any other apparent differences in the organ or myocyte structure in all 3 groups of knockout mice, indicating that the early mortality of dKO mice was not due to gross defects in cardiac architecture. Similarly, no localized areas of necrosis or myocyte damage were detected in the dKO sections.

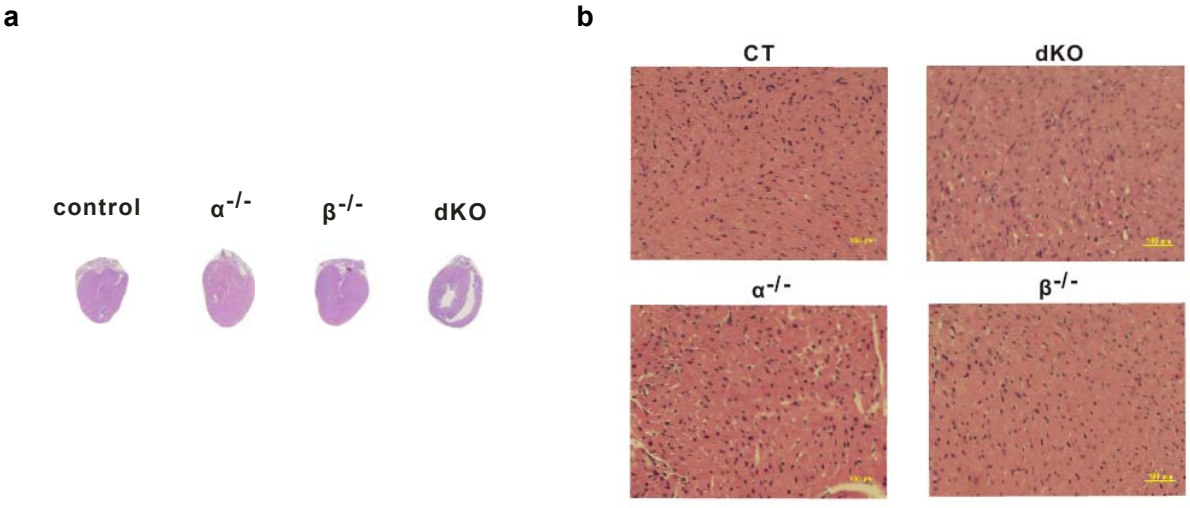

Fig. 2-2 Histology of the hearts. (**a**) Gross morphology of representative hearts from each group of mice. Sections were stained with H&E. Note the dilated ventricular chambers in the dKO heart. (**b**) Representative paraffin-embedded heart sections of control, dKO, $\alpha^{-/-}$ and $\beta^{-/-}$ mice stained with H&E.

2-3-2 Disrupted Cardiac Dyad and T-tubule Network in PI3K Knockout Myocytes

We next examined the ultrastructure of dKO myocytes in heart sections by electron microscopy. At a low magnification, the myofibril organization and sarcomere structure appeared unperturbed in the dKO myocytes (Fig. 2-3a). Closer inspection at a higher magnification showed that cardiac dyads in the dKO myocytes were not as well developed as those seen in the control myocytes. Many of the T-tubules in the dKO myocytes were not juxtaposed to jSR. For those that were, the region of contact between the jSR and T-tubule was much shorter than in control myocytes (Fig. 2-3b). We also noticed unusual dense particles deposited around the dyad in the dKO myocytes (Fig. 2-3b).

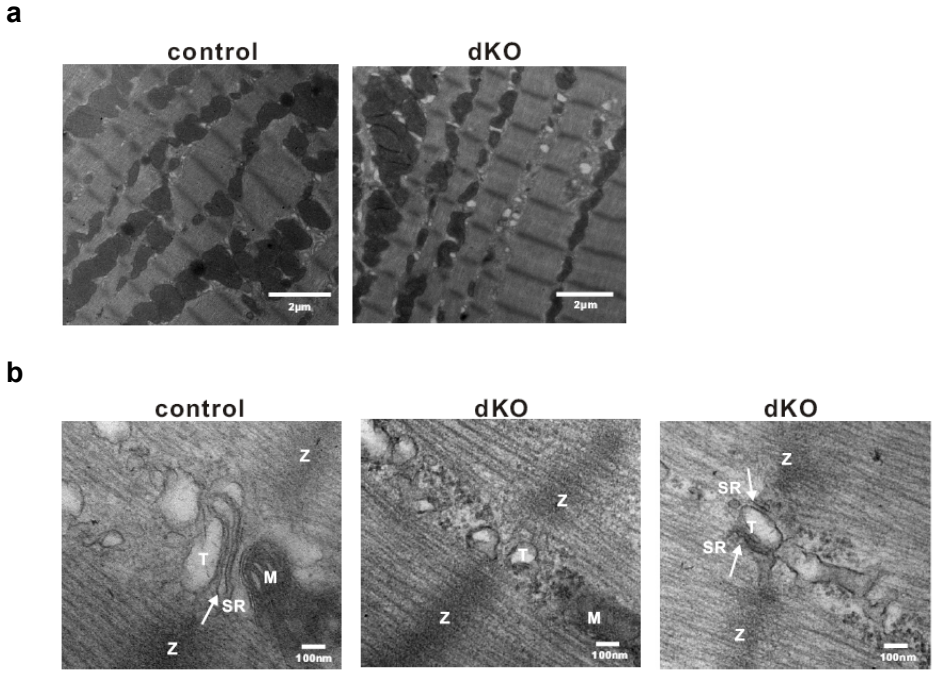

Fig. 2-3 Ablation of both p110α and p110β in cardiac myocytes causes cardiac dyad disruption. (**a**) Electron micrographs of thin sections of control and dKO left ventricular myocardium. At this magnification, the sarcomere structure and myofibril organization appear intact in the dKO cardiac myocytes. (**b**) At higher magnification, the sarcoplasmic reticulum (SR, arrow) has limited contacts with T-tubules (T) in the dKO heart, whereas they are closely aligned in the control heart. Z, Z-line; M, mitochondria.

To determine if the organization of T-tubules is affected by the loss of PI3Ks, we isolated cardiac myocytes from control, $\alpha^{-/-}$, $\beta^{-/-}$, and dKO mice, stained them with the membrane dye di-8-ANEPPS, and imaged the cells by confocal microscopy. This lipophilic dye cannot enter the cell and stains the cell surface membrane to reveal the T-tubule structure. Staining of representative myocytes from each group of mice is presented in Fig. 2-4a. In control, $\alpha^{-/-}$, and $\beta^{-/-}$ myocytes, the T-tubule network exhibited a highly organized striated pattern. The degree of spatial periodicity was quantified using 1D Fourier analysis of the di-8-ANEPPS signal along the longitudinal axis. Periodic T-tubule spacing of about 2 μm (0.5 μm^{-1} dominant spatial frequency, with a harmonic at 1 μm^{-1}) was seen in control cells (Fig. 2-4b), commensurate with the sarcomere spacing visible in the phase contrast images. In contrast, the T-tubule network in dKO myocytes was severely disrupted and the striated pattern was almost completely lost (Fig. 2-4a). There was no discernable dominant frequency in the Fourier spectrum (Fig. 2-4b), despite normal sarcomere appearance in the phase contrast images (Fig. 2-4a). This result suggests that the T-tubule disruption is probably not due to damage of dKO cells during the isolation procedure. A normalized output of the Fourier transform (power ratio of the dominant frequency peak power and low frequency noise 0.2-0.4 μm^{-1}) revealed a statistical difference in the spatial organization of the T-tubules between the control and dKO groups while both single knockouts were not significantly different from the control (Fig. 2-4c).

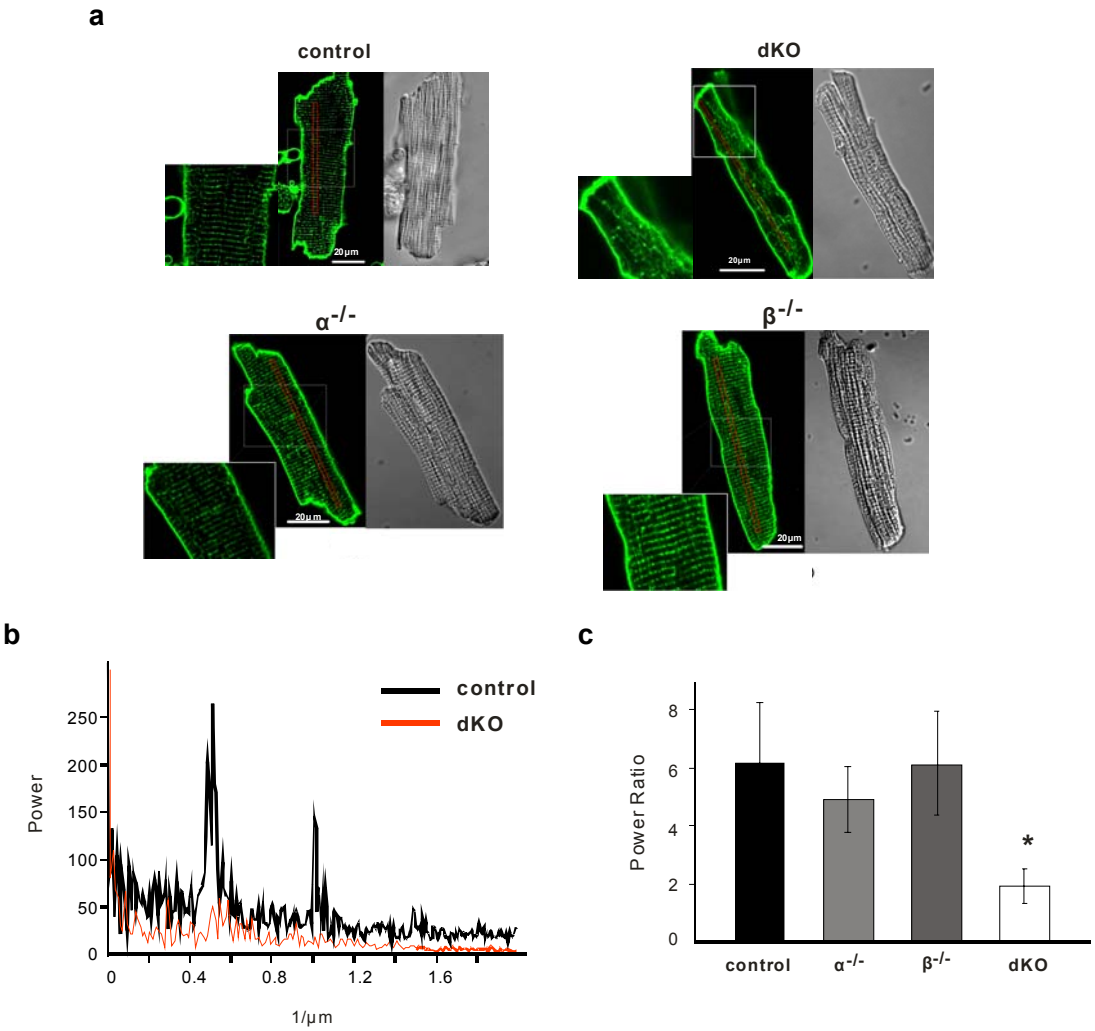

Fig. 2-4 T-tubule disruption in PI3K dKO myocytes. (**a**) Representative staining patterns seen in cardiac myocytes isolated from 35-37 days old control, $\alpha^{-/-}$, $\beta^{-/-}$ and dKO mice, stained with 10 μM di-8-ANEPPS and imaged by confocal microscopy. The small panels on the left are 2x magnified views of the boxed areas. Phase contrast images of the same cells are displayed on the right, indicating preserved sarcomere organization in all cases. (**b**) Spectrum power vs. spatial frequency along the longitudinal axis was computed using 1D Fourier analysis in the regions of interest shown in red rectangles in **a**. Control myocytes exhibited average T-tubule spacing of 2 μm (see peak at 0.5 μm^{-1} spatial frequency) whereas dKO myocytes did not display a consistent spatial frequency. (**c**) Power ratio (=$Power_{peak}$/Average($Power_{0.2\sim0.4\ \mu m^{-1}}$)) was computed as a normalized measure of spatial organization from 8-12 cells (from >3 hearts in each group). Data shown are mean with 95% confidence intervals; asterisk indicates $P < 0.05$, one-way ANOVA with *post-hoc* Fisher's test.

We next examined whether loss of both p110α and p110β changed the relative positioning of the LTCC and the RyR, two core proteins located at the cardiac dyad. Immunolabeling of isolated ventricular myocytes from control mice with antibodies to the LTCC ($Ca_V1.2$ forms the ion channel of the LTCC, green) and the RyR (red) showed that the two proteins colocalized (yellow) in highly organized striations (Fig. 2-5a, upper panels). In dKO cardiomyocytes, the LTCC pattern was disrupted and colocalization between the LTCC and the RyR or *vice versa* was markedly reduced (Fig. 2-5a, lower panels and Fig. 2-5b). Each of the LTCC and RyR spatial signals was analyzed by the Fourier transform and we found that the spatial frequencies for both were disrupted in dKO myocytes (Fig. 2-5c). Therefore, in addition to the obvious defect in the organization of T-tubules in the dKO myocytes that leads to mislocalization of the LTCC, there are also more subtle changes in the structure of the jSR where the RyRs are located.

a

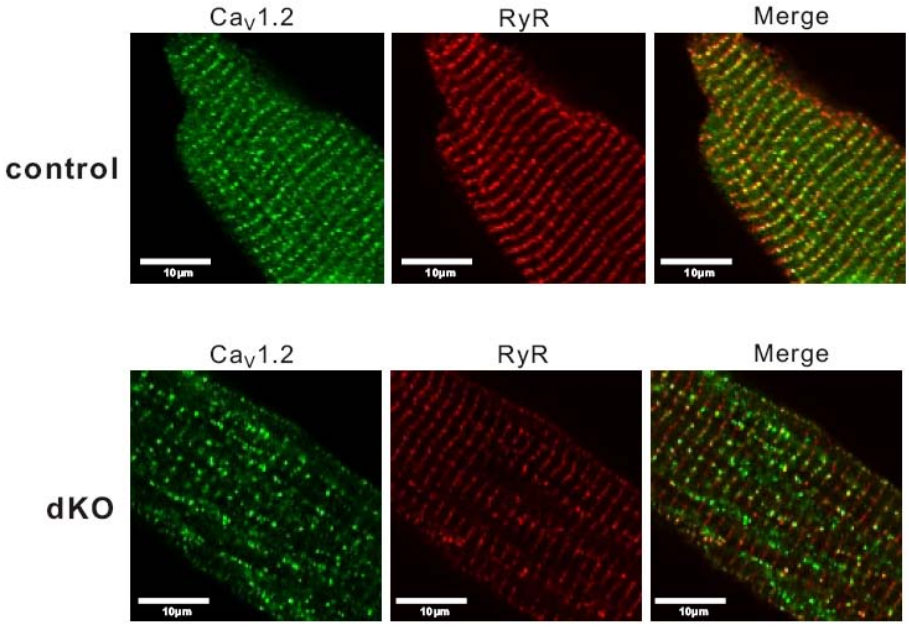

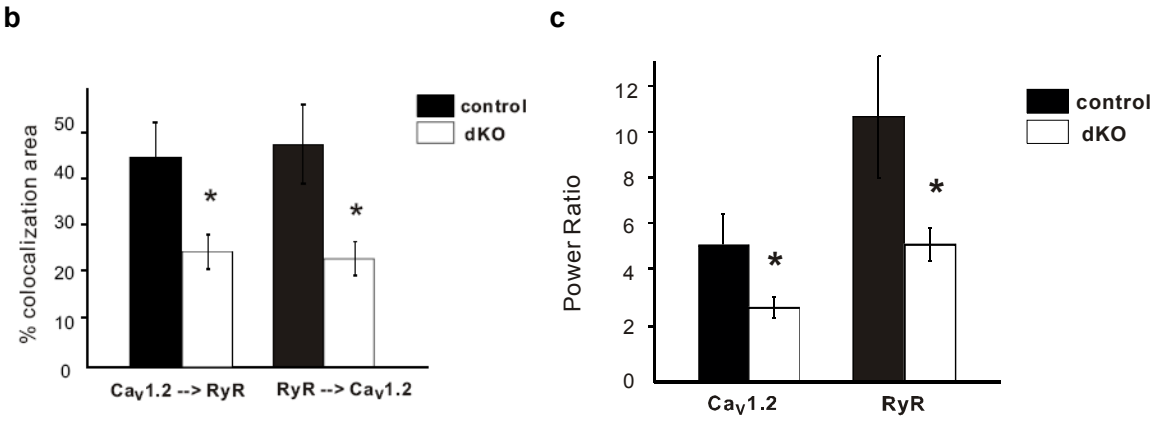

Fig. 2-5 L-type Ca^{2+} channel/ryanodine receptor mismatch in PI3K dKO myocytes. (**a**) Isolated ventricular myocytes from 35-37 days old control and dKO mice were fixed, colabeled with antibodies against $Ca_V1.2$ (green) and the ryanodine receptor (RyR, red), and imaged by confocal microscopy. (**b**) Colocalization analysis of $Ca_V1.2$ with RyR in control and dKO myocytes. Data shown are mean ± 95% confidence interval. N = 19-25 cells from 3 hearts. Asterisk indicates $P < 0.01$, t-test. (**c**) Power ratio (indicating spatial organization of $Ca_V1.2$ and RyR) was computed from 14-15 cells (from 3 hearts in each group). Data shown are mean ± 95% confidence intervals; asterisk indicates $P < 0.01$, t-test.

2-3-3 Reduced Myocyte Contractility and Ca^{2+} Transients

We next investigated the consequences of these defects in T-tubule and jSR organization on myocyte contractility and Ca^{2+} handling. These experiments were done using ventricular myocytes isolated from 35-day old mice. At this age, dKO mice did not exhibit apparent distress and were outwardly indistinguishable from control littermates. However, more than 90% of the dKO myocytes did not contract when electrically stimulated, and those that did contract did so poorly. In contrast, the majority of control myocytes were visibly contracting under the same conditions. Myocyte contractile function was quantified by measuring changes in sarcomere length in visibly contracting cells. Contractility of the dKO myocytes was dramatically reduced by 71% as compared to control cells (Fig. 2-6a, b). Myocyte contractility was decreased by 38% in $\alpha^{-/-}$ myocytes

but unaffected in $\beta^{-/-}$ myocytes (Fig. 2-6a, b). Considering the direct control of cardiac contractility by intracellular calcium levels, we next measured Ca^{2+} transients in ventricular myocytes isolated from all four groups of mice. The dKO myocytes exhibited Ca^{2+} transient amplitudes that were only 25% of control values (Fig. 2-6c, d). The decrease in peak amplitude is probably underestimated because the diastolic Ca^{2+} concentration was reduced by ~50% in the dKO myocytes (data not shown). Ablation of p110α alone caused a more moderate decrease (48% of control) in Ca^{2+} transient amplitude, whereas ablation of p110β had no effect on Ca^{2+} transients (Fig. 2-6c, d).

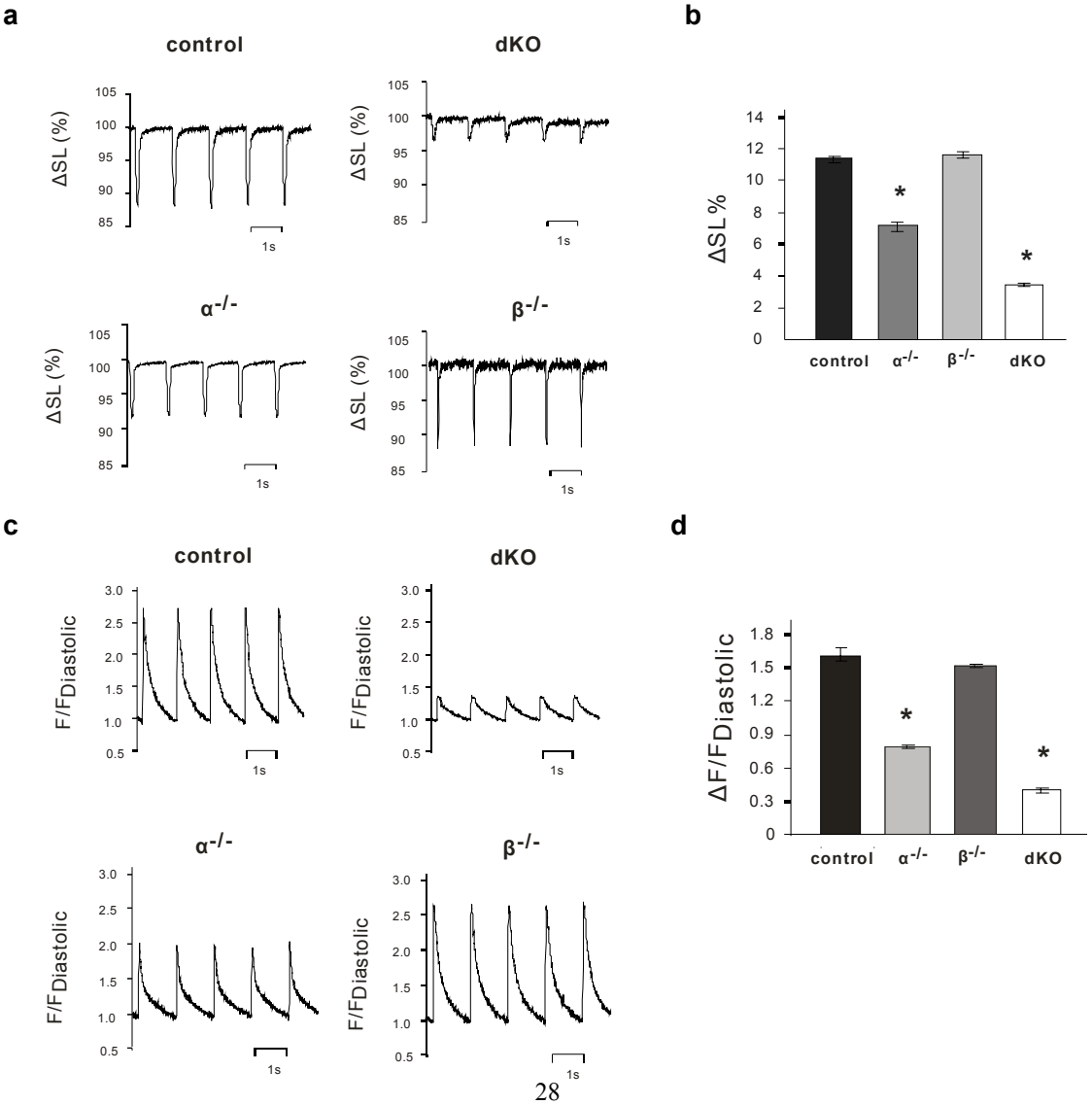

Fig. 2-6 dKO myocytes have defective contractile function. (**a**) Representative contractility tracings measured as % change in sarcomere length (ΔSL%) recorded from control, $\alpha^{-/-}$,$\beta^{-/-}$ and dKO myocytes. (**b**) Summary data of myocyte contractility measurements. Control, N = 25; $\alpha^{-/-}$, N = 10; $\beta^{-/-}$, N = 14; dKO, N = 22. (**c**) Representative Ca^{2+} transient tracings from control, $\alpha^{-/-}$,$\beta^{-/-}$ and dKO myocytes. Ca^{2+}-associated fluorescence (F) was normalized to each tracing's own minimum fluorescence ($F_{Diastolic}$). (**d**) Summary data of Ca^{2+} transient amplitudes measured in control (N = 13), $\alpha^{-/-}$ (N = 10), $\beta^{-/-}$ (N = 6) and dKO (N = 17) myocytes. Values in (**b**) and (**d**) are means ± S.E.M. Asterisk indicates comparison of the indicated group to the control group, $P < 0.05$, one-way ANOVA with *post-hoc* Fisher's test.

The triggering event in calcium release and subsequent contraction of cardiomyocytes is the Ca^{2+} influx via the LTCC. We used whole cell patch clamp techniques to show that Ca^{2+} current through the LTCC ($I_{Ca,L}$) was reduced in dKO myocytes to 50% of control values (Fig. 2-7a, b). The $\alpha^{-/-}$ myocytes displayed a 30% decrease in $I_{Ca,L}$ as compared to controls, whereas $I_{Ca,L}$ was not affected in $\beta^{-/-}$ myocytes (Fig. 2-7a, b). Finally, to test if the blunted Ca^{2+} transients in dKO cells might also be due to decreased SR Ca^{2+} stores, contracting myocytes were rapidly perfused with caffeine to release SR Ca^{2+}. The SR Ca^{2+} content in dKO myocytes was calculated to be 35% lower than in control cells (Fig. 2-7c, d). We believe that this is an underestimate of the actual decrease in SR Ca^{2+} content in dKO cells because we could not study the non-contracting cells. In summary, disruption of the cardiac dyad structure in dKO myocytes leads to severe defects in multiple aspects of Ca^{2+} handling and contractility.

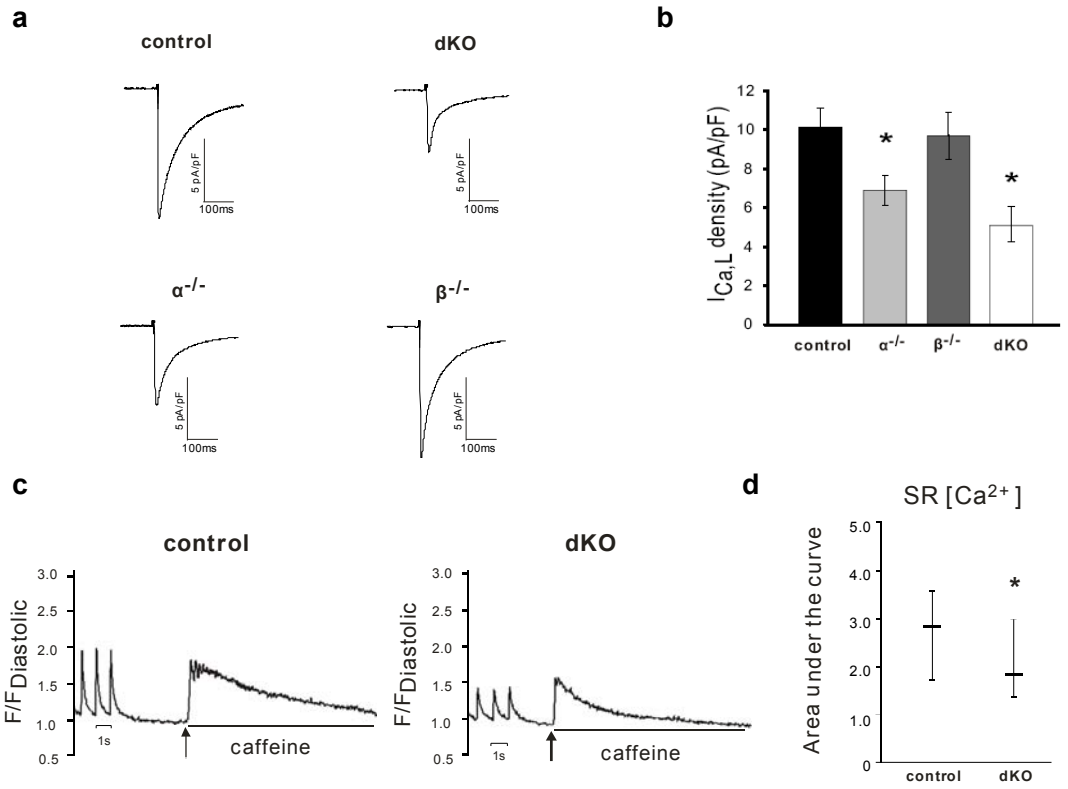

Fig. 2-7 dKO myocytes exhibit severely defective excitation-contraction coupling. (**a**) Representative recordings of L-type Ca^{2+} currents ($I_{Ca,L}$) from control, $\alpha^{-/-}$, $\beta^{-/-}$ and dKO myocytes. (**b**) Summary data of $I_{Ca,L}$ density measured at +10 mV for control (N = 16), $\alpha^{-/-}$ (N = 16), $\beta^{-/-}$ (N = 16) and dKO (N = 16) myocytes. Values are means ± S.E.M. Asterisk indicates comparison of the indicated group to the control group, $P < 0.05$, one-way ANOVA with *post-hoc* Fisher's test. (**c**) Representative Ca^{2+} tracings recorded from control and dKO myocytes following rapid caffeine (10 mM) treatment. Cells were paced at 1 Hz prior to stimulation (arrow) and caffeine treatment was throughout the whole peak. (**d**) Summary data of the area under the curve (see **c**) as an estimate of the total SR Ca^{2+} content. Values are median ± 25 percentile. Asterisk indicates $P < 0.05$, Wilcoxon rank-sum test. Control, N = 19; dKO, N = 25.

2-3-4 Decreased Expression of Cardiac Dyad Proteins

To better understand the molecular mechanism that leads to these phenotypic changes in the dKO myocytes, we investigated the expression of proteins in the cardiac dyad that control Ca^{2+} entry, release and uptake. Using real-time RT-PCR and western blotting, we found that both $Ca_V1.2$ mRNA and protein were decreased in dKO hearts as

compared to control hearts (Fig. 2-8). mRNA and protein levels of RyR, triadin and SERCA2 were also decreased (Fig. 2-8). The junctin mRNA level was significantly reduced. The mRNA level for CSQ2 was not significantly different between control and dKO myocytes, but protein expression was lower in the dKO (Fig. 2-8). This could be caused by decreased levels of triadin and junctin that bind to CSQ2 so that less of this protein is present at the SR membrane. However, expression of JP-2, which is believed to target T-tubules to the jSR, was not affected at the mRNA or protein level. The level of caveolin-3 protein, which is concentrated at T-tubules, also remained unchanged (Fig. 2-8b). Finally, we found that the mRNA level of β-myosin heavy chain (MHC) was dramatically increased in dKO hearts (Fig. 2-8b). The expression shift from α- to β-MHC is an indicator of defective cardiac contractility[95], suggesting that the early lethality in dKO mice might be due to severe contractile damage, most likely caused by defective Ca^{2+} release units on the cardiac dyads. None of the mRNA level changes in single knockout hearts was statistically significant (Fig. 2-8a). We also did not detect consistent changes in the level of these Ca^{2+}-handling proteins in the single knockouts (Fig. 2-8b), pointing to a synergistic role of the PI3K isoforms in regulation of the Ca^{2+} handling machinery.

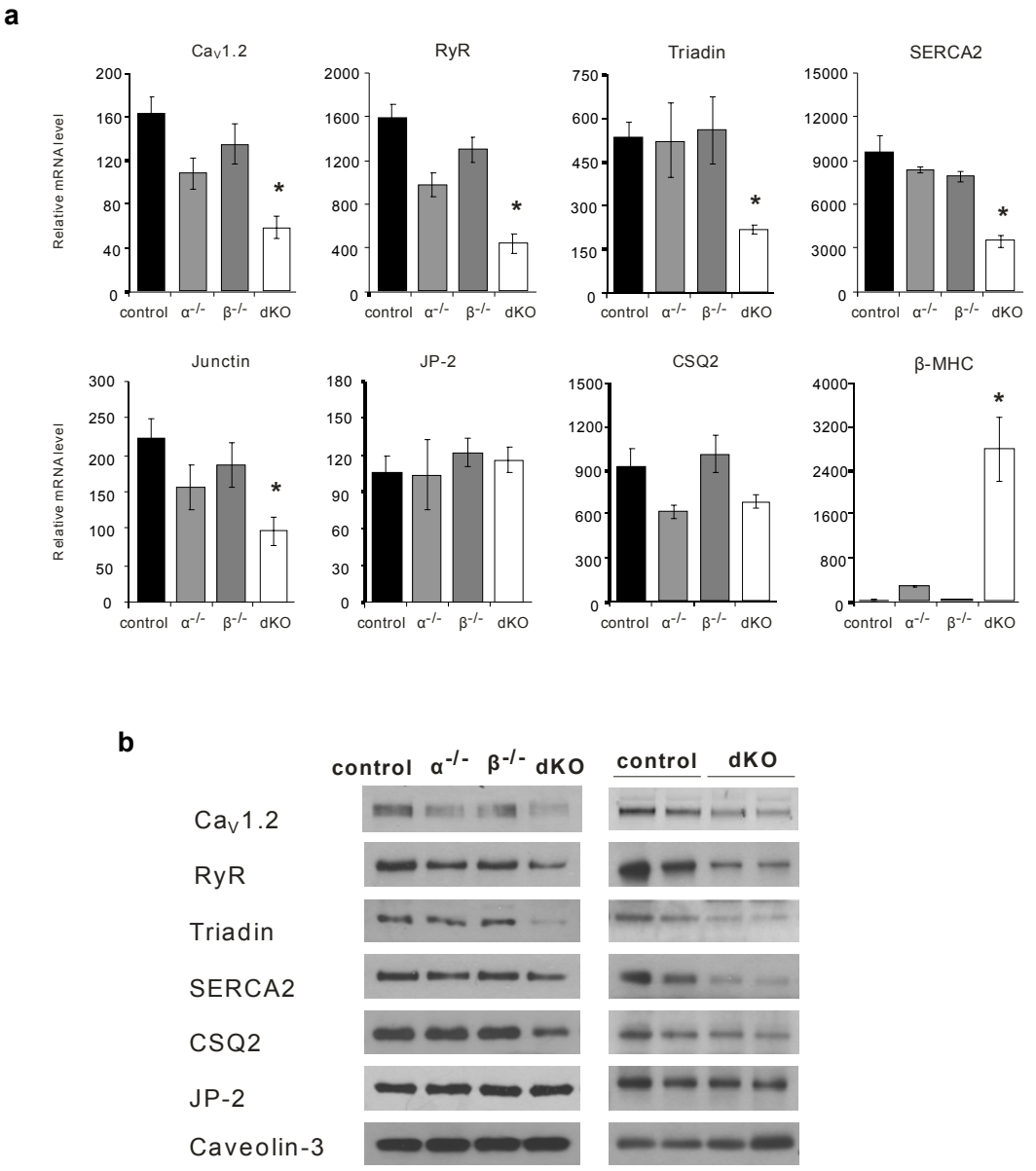

Fig. 2-8 Decreased expression of proteins located at the T-tubule/jSR junction. (**a**) Real-time RT-PCR analysis of mRNA levels of indicated genes in control, $\alpha^{-/-}$, $\beta^{-/-}$ and dKO hearts. RyR, Ryanodine receptor 2; CSQ2, calsequestrin 2; JP-2, Junctophilin-2. Asterisk indicates comparision of the indicated group to the control group, $P < 0.05$, one-way ANOVA with *post-hoc* Fisher's test. (**b**) Immunoblots of microsomal preparations obtained from control,$\alpha^{-/-}$, $\beta^{-/-}$ and dKO hearts. The left panel is one set of samples from the indicated groups. The right panel is another set with 2 control and 2 dKO samples from different animals.

2-4 Discussion

Cardiac excitation-contraction coupling is dependent on efficient Ca^{2+}-induced Ca^{2+} release[96]. This process relies upon the proper relative positioning of cell membrane components with respect to the SR, i.e., the LTCC, RyR and other proteins are found in stable structures within the cardiac dyad that allow them to act in a coordinated fashion. In this study, we provide the first genetic evidence that two ubiquitous Class IA PI3Ks, p110α and p110β, play pivotal roles in regulating cardiac contractile function by affecting the expression of multiple Ca^{2+}-handling proteins, including $Ca_V1.2$, RyR, triadin, junctin and SERCA2. Furthermore, these two kinases regulate the organization of the T-tubule network and jSR that determines the relative positioning of the LTCC and the RyR.

Currently, it is believed that JP-2-mediated targeting of jSR to plasma membranes is the initiating step that docks T-tubules to the SR[88]. Ablation of JP-2 disrupted the junctional membrane complex formation in cardiac myocytes, resulting in asynchronous Ca^{2+} transients and embryonic death[87]. We did not detect a change in JP-2 expression in the dKO hearts, so disruption of the T-tubule network in the dKO myocytes is probably not due to loss of JP-2. On the other hand, we did not rule out the possibility that JP-2 might be improperly positioned in the dKO myocytes, leading to mistargeting of the T-tubules. If disruption of the T-tubule structure leads to decreased expression of proteins at the cardiac dyad, analysis of $Ca_V1.2$, RyR and SERCA2 levels in the JP-2-null hearts could be informative. Conversely, the structural changes in the dKO myocytes could be a consequence of decreased expression of certain Ca^{2+}-handling proteins at the cardiac dyad. Ablation studies in mice suggest considerable variation in the roles of these proteins in regulating cardiac function. Myocytes lacking triadin had a marked reduction in the

extent of contacts between T-tubules and the jSR and showed decreased expression of RyR, junctin, JP-2 and CSQ2[84]. These phenotypes are similar to those of our dKO mice, but the triadin-null mice exhibited increased cardiac contractility. Ablation of the CSQ2 gene decreased expression of triadin and junctin but did not affect myocyte contractility[86]. Ablation of junctin did not decrease cardiac contractility or the expression of other Ca^{2+}-handling proteins[85]. Therefore, the contractile defect exhibited by the dKO myocytes is probably not caused by decreased levels of junctin and CSQ2. Deletion of the RyR2[97], $Ca_V1.2$[98] or SERCA2[99] genes caused embryonic lethality but the organization of the T-tubule network or expression of other Ca^{2+}-handling proteins were not examined.

Genetic deletion of signaling molecules downstream of PI3Ks can also lead to dramatic cardiac phenotypes. The PI3K/Akt signaling pathway is known to inactivate transcription factors in the FOXO family. Transgenic expression of a FOXO1 mutant that cannot be inactivated by Akt phosphorylation led to embryonic lethality due to heart failure[100]. It would be interesting to determine if FOXO transcription factors suppress the expression of $Ca_V1.2$, RyR, triadin, SERCA2 or junctin and if the nuclear localization of FOXO proteins is increased in the dKO myocytes. Ablation of both Akt1 and Akt2 led to perinatal death due to severe growth defects in multiple organs[58], and deletion of phosphoinositide-dependent kinase 1 (PDK1) in cardiac myocytes resulted in heart failure and lethality between 5-11 weeks of age[101]. It would be interesting to examine the contractility, T-tubule structure, and expression of Ca^{2+}-handling proteins in myocytes prepared from PDK1-null or Akt1/2-null mice.

We previously reported that inducible deletion of p110α, but not p110β, in myocytes of adult mice caused a reduction in contractility, Ca^{2+} transients and $I_{Ca,L}$[65]. Similar results were seen here in young animals that lacked p110α or p110β during cardiac development.

Interestingly, cardiac-specific overexpression of a constitutively active p110α mutant in adult mice increased cardiac contractility and expression of $Ca_V1.2$, RyR and SERCA2, suggesting that p110α might positively regulate these genes[102]. However, we did not detect significant decreases in the mRNA levels of these genes in $\alpha^{-/-}$ hearts. Up to now, minimal cardiac phenotype has been detected in the $\beta^{-/-}$ mice described here. The severity of the phenotype in dKO mice as compared to the single knockouts suggests that p110α and p110β might have different functions in the heart and that both are required for establishment of functional Ca^{2+} release units. The specific contribution of p110β to cardiac development is under investigation.

In conclusion, we have demonstrated that the presence of p110α and p110β is crucial for maintaining normal heart function. The loss of both PI3K isoforms led to Ca^{2+} handling abnormalities mediated by improper assembly of the cardiac dyads in cardiac myocytes that resulted in early death. These results may have clinical implications for the use of PI3K inhibitors in patients with diseases such as cancer.

Chapter 3

Differential Regulation of Skeletal Muscle Mass by p110α and p110β

3-1 Introduction

Skeletal muscle is the most abundant tissue in the human body, accounting for about 50% of the body mass. Therefore, the maintenance of its size or mass is essential to ensure basic functions such as metabolism and locomotion[103]. Muscle atrophy is defined as a decrease in the mass of the muscle and the loss can be either localized or throughout the body. It is associated with numerous diseases such as cancer and AIDS[104]. There are also some other situations which can cause atrophy; for instance, in patients with prolonged illness requiring extended bedrest, the inactivity leads to rapid muscle loss. Even during normal aging, there is gradual loss of muscle mass. Hypertrophy of skeletal muscle, on the other hand, is characterized by an increase in the size of myofibers. It occurs as an adaptive response to load-bearing exercise and as a result of an enhanced rate of protein synthesis[105]. There are compelling reasons to develop new medicines to maintain muscle mass. Therefore, understanding the mechanisms of how muscle mass is regulated might aid in the identification of novel targets for anti-atrophy drug discovery. Potential treatments for muscle atrophy could either block protein degradation pathways or stimulate protein synthesis pathways.

The mTOR pathway has emerged as a key regulator of protein synthesis and growth in many cell types[106-108]. As discussed in Chapter 1, mTOR exists in two distinct multi-protein complexes, mTORC1 and mTORC2. Depending on the partners in the

complex, mTOR phosphorylates distinct substrates. Raptor in the mTORC1 complex directs mTOR to phosphorylate S6K, which regulates protein synthesis by phosphorylating ribosomal protein S6 and other proteins in the translation machinery[109]. IGF-1 is a critical hormone in regulating muscle mass. IGF-1 induces hypertrophy by stimulating the PI3K/Akt pathway, resulting in the downstream activation of mTOR pathways[110]. In addition, mTOR/S6K integrates signaling pathways from AMP-activated protein kinase (AMPK)[111], amino acids[112-113], and other nutrients[114].

It is believed that the PI3K/Akt pathway not only activates the mTOR pathway to promote muscle hypertrophy, but also prevents muscle atrophy by inhibiting FOXOs [115-116]. FOXO transcription factors regulate the expression of E3 ubiquitin ligases atrogin-1/MAFbx (muscle atrophy F-box)[117] and MuRF-1 (muscle ring finger-1)[118] to induce muscle atrophy. Akt phosphorylation of FOXOs inhibits their translocation to the nucleus and blocks FOXO-induced upregulation of atrogin-1 and MuRF-1.

Recent studies have shown that mice expressing whole-body kinase-dead knockin mutants of either p110α or p110β have growth retardation[18, 56]. Deletion of p85 regulatory subunits specifically in the muscle also impairs muscle growth[119]. These results suggest that Class IA PI3Ks are important for regulating muscle mass. Therefore, I investigated the regulation of skeletal muscle mass by p110α and p110β regulates and this chapter describes the findings from these studies. The same knockout mouse models of p110α and p110β that were described in Chapter 2 were used in these studies. I also investigated muscle-specific PTEN-null mice to determine if upregulation of PI3K signaling and downregulation of PI3K signaling would yield opposite muscle phenotypes. Lastly, I investigated if the effects of PTEN loss on muscle mass could be reversed by simultaneously deleting either p110α or p110β with PTEN.

3-2 Materials and Methods

General Materials

Antibodies were purchased from commercial sources: p110α from BD Biosciences; p110β, p110δ, IRS-1, Akt and S6K from Santa Cruz Biotechnology; pan-p85 from Millipore; and PTEN, phospho-T308-Akt and phospho-T389-S6K from Cell Signaling. Western blot signals were visualized using horseradish peroxidase-linked secondary antibodies (Amersham Biosciences).

Cryosection Preparation and Staining

Gastrocnemius muscles were dissected and embedded in Tissue Freezing Medium (Triangle Biomedical Sciences) in liquid nitrogen-cooled isopentane. Sections of 8 μm thickness were cut and stained with hematoxylin and eosin.

MicroCT Scanning

Mice were anesthetized by 1% isoflurane inhalation and positioned with the left hind leg fully extended. The area from the end of tibia to half of the femur was scanned at an isotropic voxel size of 82 μms (70 kV, 114 μA, 300 ms integration time) with a vivaCT75 scanner (Scanco Inc, SUI). Two-dimensional gray-scale image slices were reconstructed into a three-dimensional tomography. The region of interest for each animal was defined based on skeletal landmarks from the gray-scale images. A custom script written in image processing language with the help of the Dr. Stefan Judex lab was used to analyze total muscle volume[120].

Kinase Assays

PI3K activity assay

Gastrocnemius muscle lysates (1 mg protein) in RIPA buffer (50 mM Hepes, pH 7.5,

50 mM NaCl, 50 mM NaF, 5 mM EDTA, 1 mM Na_3VO_4, 10 mM $Na_4P_2O_7$, 5% Na deoxycholate, and 10% NP-40) plus protease inhibitors were incubated with 1 μg of IRS-1 antibody at 4˚C overnight or for 3 hr and then with 25 μl of protein A-agarose (Roche) for 1 hr. Beads were washed twice with RIPA buffer and twice with PI3K assay buffer (20 mM Hepes, pH 7.5, 100 mM NaCl, and 50 mM EDTA). The immunocomplexes were assayed for PI3K activity[121].

S6K activity assay

Gastrocnemius muscle lysates (250 μg protein) in IP buffer (50 mM Tris, 120 mM NaCl, 20 mM NaF, 1 mM benzamidine, 5 mM EGTA, 30 mM $Na_4P_2O_7$, 1% Triton X-100, 30 mM p-nitrophenyl phosphate (PNPP), and 0.5 mM DTT, pH 7.2) plus protease inhibitors were incubated with 1 μg of S6K antibody at 4˚C for 3 hr and then with 25 μl of protein A-agarose (Roche) for 1hr. Beads were washed twice with IP buffer and twice with low DTT S6K assay buffer (50 mM Tris, 100 μM EGTA, 10 mM $MgCl_2$, 0.1% Triton X-100, 5% ethylene glycol, 0.25 mg/ml BSA, and 500 μM DTT, pH 7.5). The washed immunocomplexes were resuspended in S6K assay buffer (50 mM Tris, 0.1 mM EGTA, 5% ethylene glycol, 0.25 mg/ml BSA, 5 mM DTT, 10 mM $MgCl_2$, and 0.1% Triton X-100, pH 7.5) containing 12 μM ATP, 2.5 μCi of [γ-^{32}P]ATP, 0.8 μM protein kinase A inhibitor peptide (Sigma), 4 mM PNPP, and 200 μg/ml S6K peptide substrate (Santa Cruz Biotechnology). The reaction mixture was incubated with 1000rpm shaking for 30 min at 37°C, and then an aliquot was spotted onto P81 phosphocellulose paper. Following extensive washing 4 times in 0.5% phosphoric acid, radioactivity on the papers was quantified by scintillation counting.

General Activity Monitoring

The general activity was measured using an LE 8811 infrared actimeter system

(Panlab s.l.). For each experiment, one mouse was put in one cage and monitored for 24 hr. Data were collected by analyzing the position and frequency with which the mice broke the infrared beams.

Hindlimb Suspension

Mice were subjected to 21 days of hindlimb unloading using a model modified from the established tail suspension model[122]. All mice were individually housed in standard cages at 24˚C and allowed free access to standard rodent chow and tap water. Weights for all animals were recorded at the beginning of the study and monitored throughout the experiment[123]. Before and after the suspension, gastrocnemius muscle volume for each mouse was monitored using a microCT scanner.

3-3 Results

3-3-1 Phenotypic Changes of Muscle p110α-Null and p110β-Null Mice

These studies used the same knockout mouse models for p110α (abbreviated as m-$\alpha^{-/-}$ hereafter) and p110β (abbreviated as m-$\beta^{-/-}$ hereafter) that were used in Chapter 2. The m-$\alpha^{-/-}\beta^{-/-}$ dKO mice were not studied because they die at a young age. The expression level of PI3Ks in the gastrocnemius muscle of m-$\alpha^{-/-}$ and m-$\beta^{-/-}$ mice was examined by western blotting. As expected, the level of p110α or p110β protein was decreased in the appropriate p110 knockout mouse strain (Fig. 3-1). Interestingly, the amounts of p110β and p85 were also decreased in the p110α knockout muscle. The large decrease of p85 may indicate that p110α is the major binding partner for this regulatory subunit in the muscle. The third class IA PI3K catalytic subunit, p110δ, was

also detected in skeletal muscle and its expression was not affected by ablation of p110α or p110β (Fig. 3-1). As a control, I also studied the muscle-specific PTEN$^{-/-}$ (abbreviated as m-PTEN$^{-/-}$ hereafter) mouse. As expected, the muscle PTEN protein level was low in the knockout mouse (Fig. 3-1).

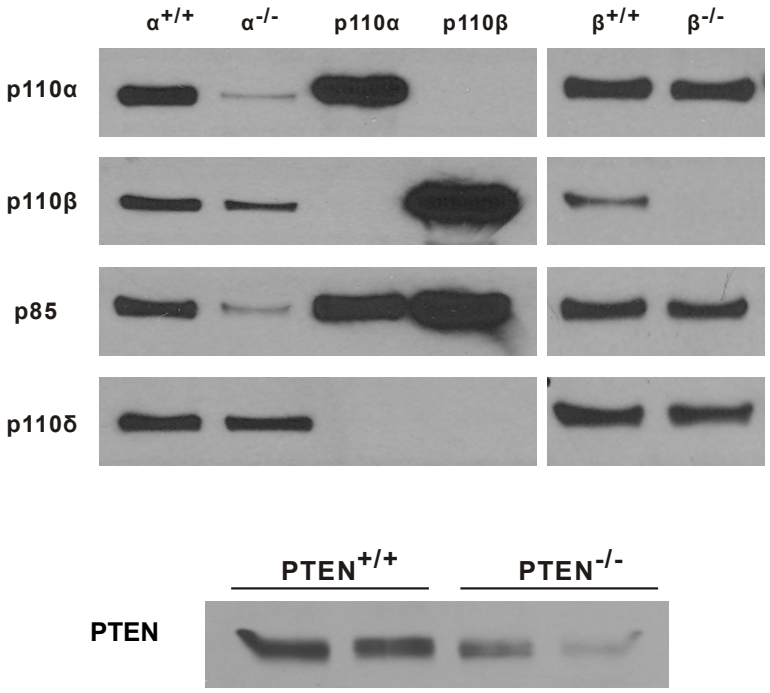

Fig. 3-1 Muscle PI3K and PTEN expression. PI3Ks in lysates prepared from gastrocnemius muscles were pulled down with a phosphotyrosine peptide coupled to agarose and then analyzed by western blotting with the indicated antibodies. Recombinant proteins p110α/p85α (p110α) and p110β/p85α (p110β) were loaded as controls. Gastrocnemius muscle lysates were analyzed by western blotting with PTEN antibody.

None of the three knockout mouse strains displayed obvious distress and they were indistinguishable from their wildtype littermates. Examination of growth curves of PI3K knockout mice showed that between 10-16 weeks of age, m-α$^{-/-}$ mice had reduced body weight as compared to their littermate controls (Fig. 3-2). However, the body weight

difference was no longer present in older animals. In contrast, average body weights of m-$\beta^{-/-}$ mice were the same as controls until 16 weeks of age (Fig. 3-2). At that time, the m-$\beta^{-/-}$ mice became heavier than their littermate controls and remained so up to 28 week of age.

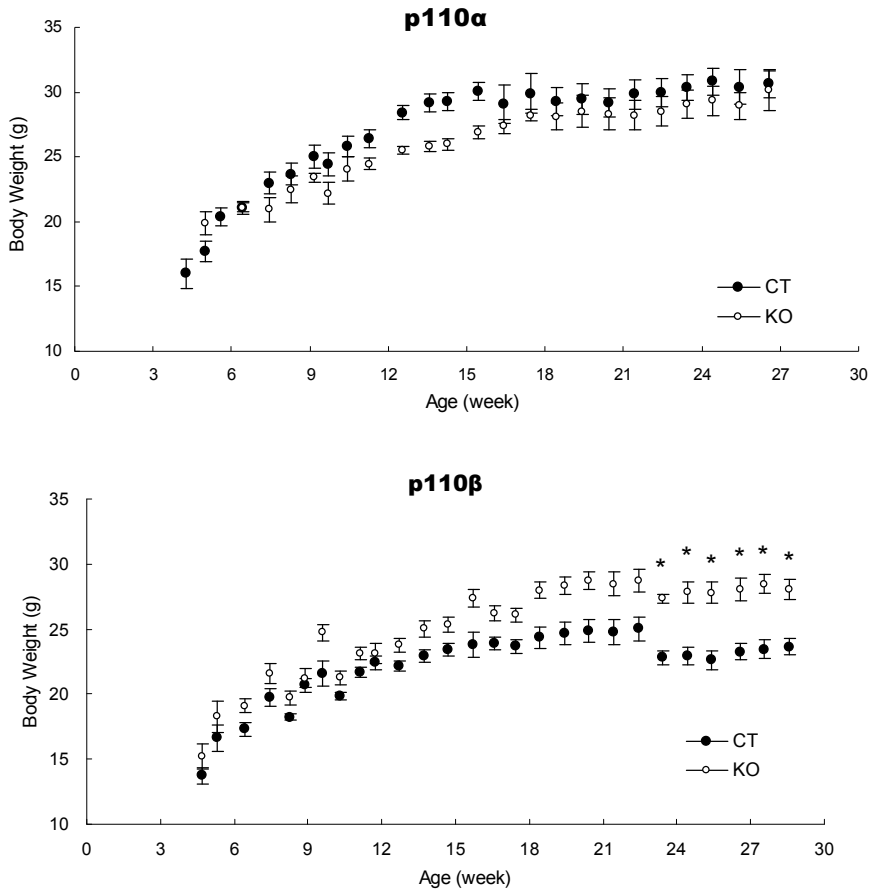

Fig. 3-2 Growth curves of m-$\alpha^{-/-}$ and m-$\beta^{-/-}$ mice. Body weights of 6 animals in each group were recorded from 4 weeks of age up to 27-28 weeks.

I used three techniques to investigate the muscle size in PI3K knockout mice. First, the hindlimbs of PI3K knockout mice were imaged using an *in vivo* microCT

scanner. All of the animals were scanned at 2 months of age. The region scanned was from the point where the tibia and fibula join together to the metaphysis area where the growth plate disappears. Cross-section CT images of the left hindlimb were then reconstructed (Fig. 3-3a). Image analysis was performed to calculate the muscle volume, which was then normalized to the tibia length (shown as muscle area). There was a statistically significant decrease (20%) in the muscle size of m-$\alpha^{-/-}$ mice as compared to their littermate controls (Fig. 3-3b). In contrast, the mean muscle size was not statistically different between m-$\beta^{-/-}$ mice and their controls. In addition, I found a significant increase (36.5%) in the muscle size of m-PTEN$^{-/-}$ mice (Fig. 3-3b).

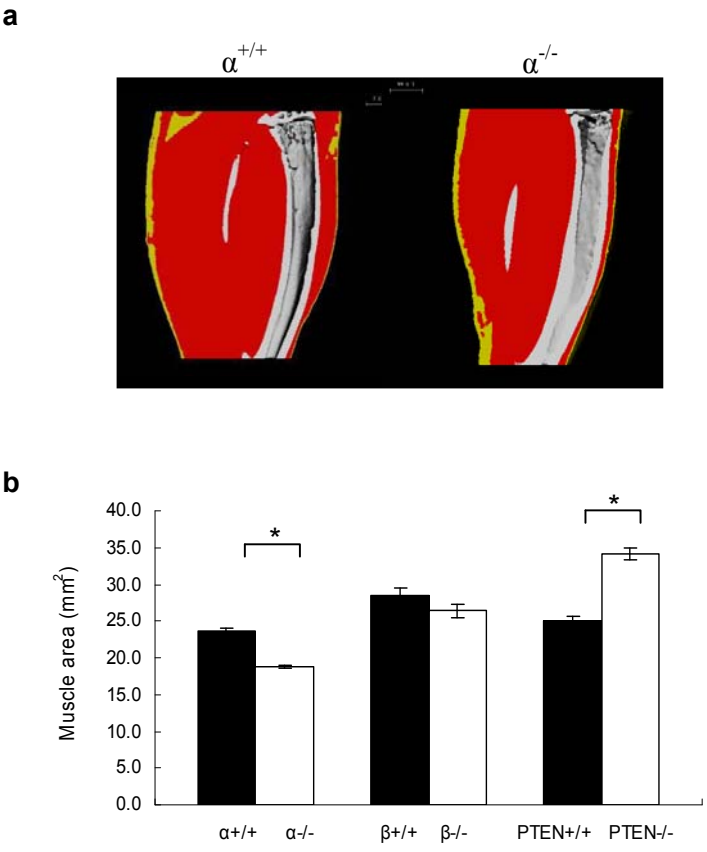

Fig. 3-3 Gastrocnemius muscle size. (**a**) Representative microCT image reconstructions labeled with

pseudo color. Red indicates muscle. (**b**) Calculated muscle volume from microCT images was normalized to the tibia length. Values are shown as mean ± S.E.M. Asterisks indicate $P < 0.001$, t-test. (m-$\alpha^{-/-}$, N = 10; m-$\alpha^{+/+}$, m-$\beta^{+/+}$, and m-$\beta^{-/-}$, N = 7; m-PTEN$^{+/+}$, N=6; m-PTEN$^{-/-}$, N = 4).

Second, gastrocnemius muscles were harvested from PI3K or PTEN knockout mouse strains and weighed. There was a significant decrease (20.7%) in the gastrocnemius muscle weight of m-$\alpha^{-/-}$ mice as compared to their control mice (Fig. 3-4a). Consistent with my findings using the microCT scanner, the mean muscle weight of m-$\beta^{-/-}$ mice was not statistically different from the control values. As expected, the average muscle weight of m-PTEN$^{-/-}$ mice was significantly increased by 38.6% (Fig. 3-4a). Finally, I examined the size of myotubes in all three knockout mouse strains. Gastrocnemius muscles were fixed, sectioned and stained with H&E. Images of muscle sections were then captured by light microscopy and a digital camera (Fig. 3-4b). Image analysis was used to determine the areas of 150-200 myotubes from each knockout and control mouse strain. Consistent with my microCT and muscle weight results, I found that the average myotube size was significantly decreased by 26.3% in m-$\alpha^{-/-}$ mice as compared to controls (Fig. 3-4c). There was no significant difference in the myotube size between m-$\beta^{-/-}$ mice and their controls. The myotube size was significantly increased by 29% in m-PTEN$^{-/-}$ mice as compared to their controls (Fig. 3-4c).

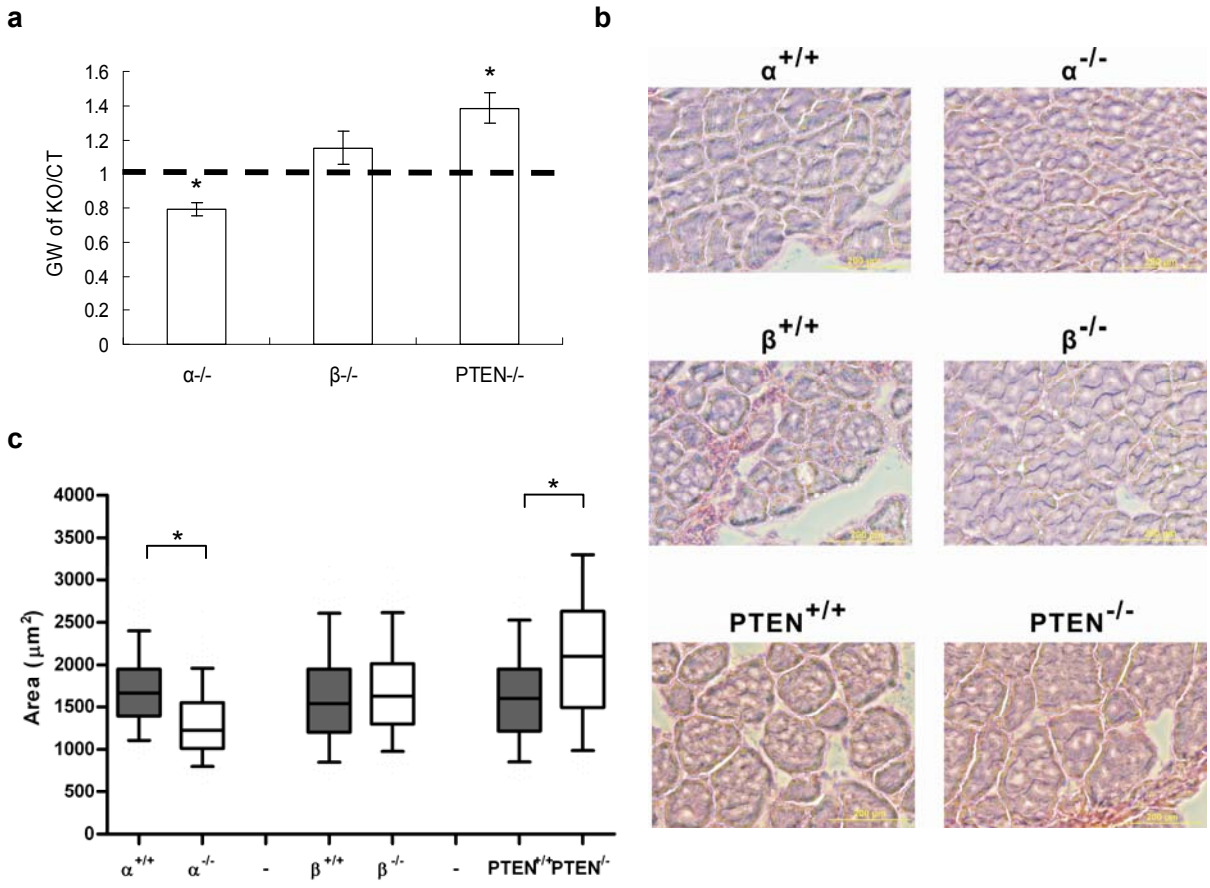

Fig. 3-4 Gastrocnemius muscle weight and myotube size. (**a**) Gastrocnemius muscles from 2-month old animals were weighed (N=3 for each group). Weights of knockout muscles were normalized to weights of control muscles. Asterisks indicate $P < 0.05$, t-test. (**b**) Represenative cryosections of the gastrocnemius muscles stained with H&E. (**c**) Cross-sectional area of myotubes was calculated using the Image J software (N = 150-200 myotubes from 9-12 sections for each mouse. Sections were prepared from 3 mice in each group). Values shown are median ± 25% percentile. Asterisks indicate $P < 0.05$, Wilcoxon rank-sum test.

3-3-2 IGF-1 Signaling in the Muscle of m-$\alpha^{-/-}$ and m-$\beta^{-/-}$ Mice

I next investigated cell signaling pathways that might be responsible for the muscle mass reduction in m-$\alpha^{-/-}$ mice. As discussed in the Introduction, PI3K activity is necessary for IGF-1-mediated hypertrophy in skeletal muscle. Therefore, I examined IGF-1 signaling in the muscles of PI3K knockout mice. Mice were fasted overnight (16 hr). The

next day, the animals were anesthetized, a midline abdominal incision was made and the inferior vena cava (IVC) was exposed. IGF-1 was then injected into the IVC and the gastrocnemius muscle was harvested 7 min later. Tissue lysates were prepared from the gastrocnemius muscle and proteins were immunoprecipitated with an IRS-1 antibody. The immunocomplex was then subjected to an *in vitro* PI3K assay. The IGF-1-stimulated increase in PI3K activity was almost completely ablated in the p110α-null muscle (Fig. 3-5a). In contrast, IGF-1 activation of PI3K was slightly higher in the p110β-null muscle than in the control (Fig. 3-5b).

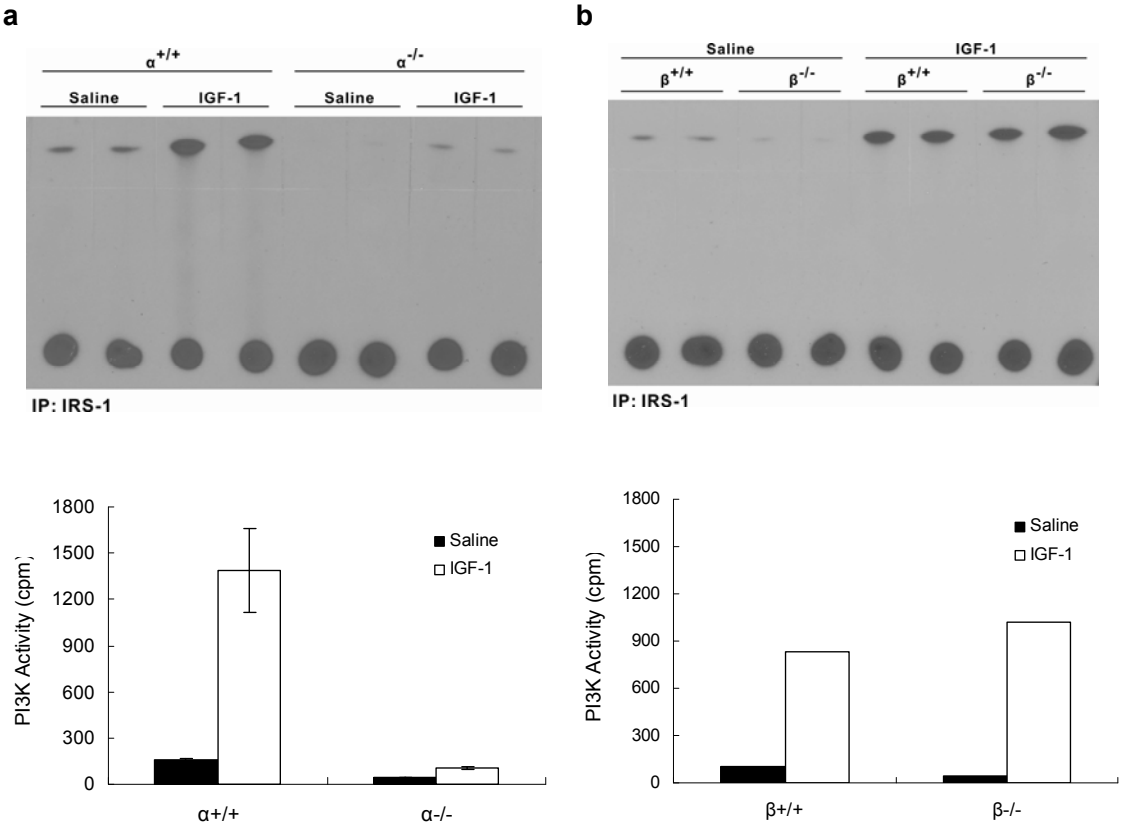

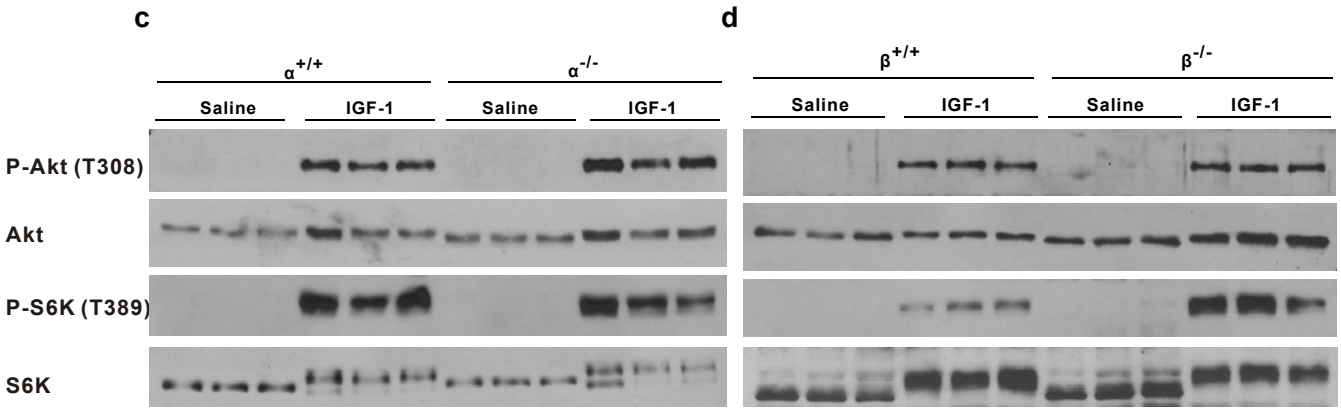

Fig. 3-5 IGF-1 activation of PI3K signaling in muscle. Anesthetized mice were injected with saline or 1 mg/kg IGF-1 through the inferior vena cava and gastrocnemius muscles were harvested 7 min later. (**a, b**) IRS-1 associated PI3K activity in the gastrocnemius muscle. Shown in the top panels are autoradiographs of representative PI3K assays. Bottom graphs are summary results from 2 experiments. (**c, d**) The same muscle lysates were analyzed by western blotting with the indicated antibodies.

Next, I examined the activation status of some downstream effectors of PI3K, namely Akt and S6K. Since both protein kinases are activated by phosphorylation, I used western blotting and phospho-specific antibodies to perform these studies. Surprisingly, I found that phosphorylation of neither Akt nor S6K was decreased in the muscle of IGF-1-treated m-$\alpha^{-/-}$ mice (Fig. 3-5c). IGF-1-stimulated Akt phosphorylation was also not affected by the loss of p110β (Fig. 3-5d). Interestingly, IGF-1 activation of S6K was greater in $\beta^{-/-}$ muscles as compared to controls (Fig. 3-5d). In summary, although IGF-1 activation of PI3K was greatly reduced in the $\alpha^{-/-}$ muscle, this did not translate into decreased Akt or S6K activation by this growth factor. These results suggest that some other downstream effector(s) of PI3K is responsible for the reduced muscle mass exhibited by the m-$\alpha^{-/-}$ mice.

3-3-3 Physiological Studies of m-$\alpha^{-/-}$ and m-$\beta^{-/-}$ Mice

To investigate if ablation of either PI3K in the muscle might have physiological consequences for the whole animal, I first examined their total physical activity level. Motor activity of these animals was monitored for 24 hours using a grid crisscrossed with infrared beams in 3 dimensions. Breaking of the beams due to physical activity by the animals was automatically recorded. As expected, control mice were most active at night (Fig. 3-6). Surprisingly, m-$\alpha^{-/-}$ mice were relatively inactive during the night time period and about as active as the control mice during the day time period (Fig. 3-6).

a

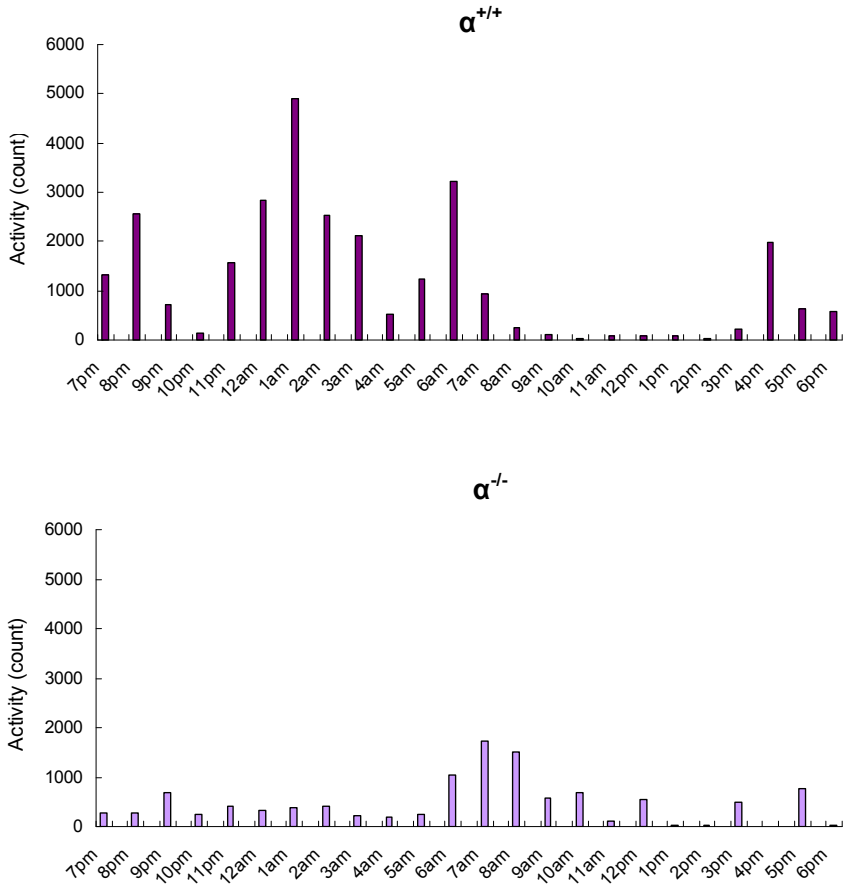

b

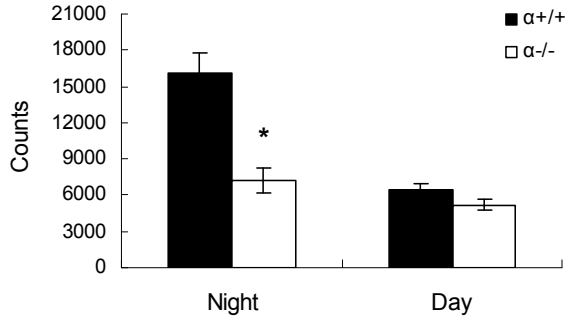

Fig. 3-6 Physical activity measurements. (**a**) Representative recordings of physical activity over a 24 h period for one control and one m-$\alpha^{-/-}$ mouse. (**b**) Summary results from 5 animals in each group. Night (7 PM-7 AM); Day (7 AM-7 PM). Values are mean ± S.E.M. Asterisk indicates $P < 0.05$, t-test.

I next investigated if ablation of either PI3K affects muscle loss due to unloading. All the mice were imaged with the microCT scanner to measure their hindlimb muscle size prior to the study. Mice were then suspended by their tails to unload the hindlimbs for 3 weeks. At that time, they were imaged again with the microCT scanner. The same animals were then removed from the suspension apparatus and allowed to move freely. After a 3 week recovery period, these animals were then imaged for the third time with the microCT scanner. As expected, mice in both control groups had decreased muscle size after 3 weeks of suspension and recovered all (m-$\alpha^{+/+}$) or some (m-$\beta^{+/+}$) of the lost muscle during the recovery period (Fig. 3-7). The m-$\alpha^{-/-}$ mice started the experiment with smaller muscles and they lost slightly less muscle than their control littermates (Fig. 3-7a). However, they also gained slightly less muscle during the recovery period. The muscle loss and recovery patterns of the m-$\beta^{-/-}$ mice were essentially the same as those exhibited by their controls (Fig. 3-7b).

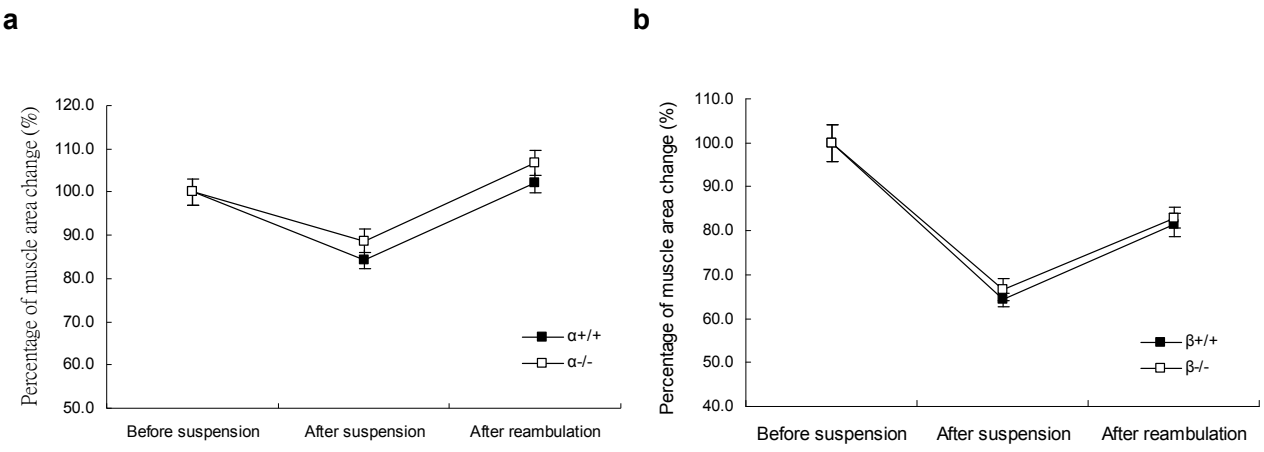

Fig. 3-7 Muscle size changes in response to hindlimb suspension. 2-month old m-$\alpha^{-/-}$ or m-$\beta^{-/-}$ mice (N = 5 in each group) and their respective controls (N = 4 or 5) were suspended by their tails for 3 weeks to unload the hindlimbs, followed by a 3-week recovery period. Data shown are muscle volumes normalized to tibia length measured with the microCT scanner. Values are mean ± S.E.M.

In conclusion, loss of p110α in both the skeletal muscle and heart dramatically affected the level of physical activity whereas loss of p110β did not have this effect. However, ablation of neither p110α nor p110β enhanced the loss of muscle mass induced by unloading.

3-3-4 Muscle Size and S6K Activity in α/PTEN Double Knockout and β/PTEN Double Knockout Mice

As discussed in the Introduction, PTEN antagonizes PI3K signaling. Current thinking is that PTEN primarily antagonizes p110β signaling to exert its function as a tumor suppressor gene[56, 71]. My next set of experiments aimed to determine if PTEN also primarily antagonizes p110β signaling to control muscle size. For this study, I generated m-$\alpha^{-/-}$;m-PTEN$^{-/-}$ and m-$\beta^{-/-}$;m-PTEN$^{-/-}$ double knockout mouse strains and compared them to their respective m-PTEN$^{-/-}$ littermate controls. Using the microCT scanner, I found

that the muscle size in m-$\beta^{-/-}$;m-PTEN$^{-/-}$ mice was slightly larger than in m-PTEN$^{-/-}$ control mice (Fig. 3-9b), suggesting that loss of PTEN does not increase muscle size by allowing an increase in p110β signaling. In contrast, the average muscle size in the m-$\alpha^{-/-}$;m-PTEN$^{-/-}$ mice appeared to be smaller than that measured in the m-PTEN$^{-/-}$ controls (Fig. 3-8a). However, the difference was not statistically significant. This may be due to the relatively small sample size and the relatively large variation in muscle size in the m-PTEN$^{-/-}$ control group. Additional animals need to be studied to conclusively determine if ablation of p110α can block the stimulatory effect of PTEN loss on muscle size.

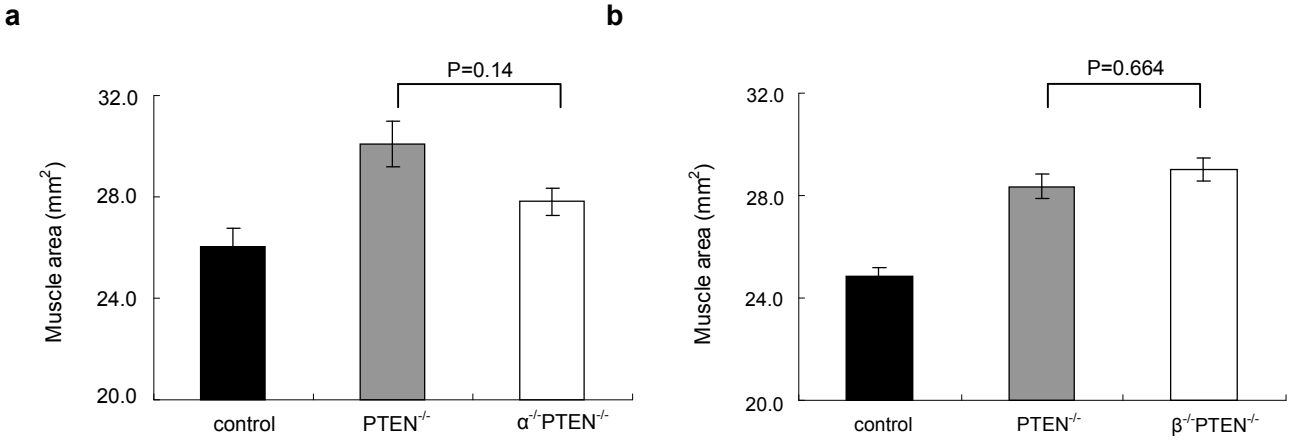

Fig. 3-8 Muscle size in m-$\alpha^{-/-}$;m-PTEN$^{-/-}$ and m-$\beta^{-/-}$;m-PTEN$^{-/-}$ double knockout mice. MicroCT scanning on the tibia region of the left hindlimbs from mice of the indicated groups was performed and the muscle volume was normalized to the tibia length. (**a**) N = 4 in $\alpha^{+/+}$PTEN$^{+/+}$ and PTEN$^{-/-}$ groups and N = 6 in $\alpha^{-/-}$PTEN$^{-/-}$ group. (**b**) N = 6 in each group. Values are shown as mean ± S.E.M.

It is well established that loss of PTEN can lead to activation of S6K in a variety of cell culture models[124]. Consistent with these reports in the literature, I found that muscle from m-PTEN$^{-/-}$ mice exhibited a 3-fold increase in S6K activity as compared to the activity measured in control muscle (Fig. 3-9). In contrast, I found that S6K activity in the

p110α-null muscle was only 31% of that in the control (Fig. 3-9). Loss of p110β did not significantly affect skeletal muscle S6K activity (Fig. 3-9). Future studies will determine if ablation of p110α can reverse PTEN$^{-/-}$-induced S6K activation using the m-α$^{-/-}$;m-PTEN$^{-/-}$ mice.

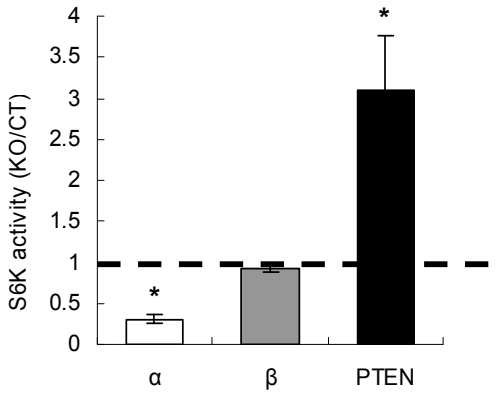

Fig. 3-9 Basal S6K activity in PTEN or PI3K knockout muscles. Gastrocnemius muscle lysates (1 mg protein each) prepared from m-α$^{-/-}$, m-β$^{-/-}$ and m-PTEN$^{-/-}$ mice and their respective controls (N = 4 for each group) were immunoprecipitated with an S6K antibody and then subjected to an *in vitro* S6K assay. Values were normalized to controls (shown as the dashed line). Asterisks indicate $P < 0.05$, t-test.

3-4 Discussion

Studies in this chapter aimed to dissect the distinct roles of p110α and p110β in regulating skeletal muscle mass. Since neither m-α$^{-/-}$ nor m-β$^{-/-}$ mice displayed any gross abnormalities at birth, this indicates that neither PI3K is essential for embryonic development of muscle. However, ablation of p110α decreased muscle mass in 2-month old animals whereas deletion of p110β did not affect muscle size. This result is consistent with my finding that IGF-1 activation of PI3K through IRS-1 is almost exclusively

mediated by p110α. Surprisingly, IGF-1 signaling to the Akt/S6K pathway was not decreased in the p110α-null muscle. These results imply that some other signaling pathway downstream of PI3K, such as atypical PKCs or small GTPases, is reponsible for IGF-1 regulation of muscle mass.

Somewhat surprisingly, loss of p110α also did not accentuate muscle atrophy in response to hindlimb unloading. This could be because Akt signaling is not downregulated in the p110α-null muscle and therefore atrophy-associated genes MuRF-1 and atrogen-1 were not upregulated (data not shown). Another possibility is that the 3-week time period might not be the ideal time point to observe the unloading-induced muscle loss. At this time point, the percentage muscle loss in the control and m-$\alpha^{-/-}$ mice was relatively small. Finally, a larger number of animals might be needed for a more conclusive study. This is especially important since these mice are not in a pure genetic background.

Finally, it was also surprising that the muscle size increase in m-PTEN$^{-/-}$ mice was not reversed by ablation of p110β because recent reports in the literature suggest that tumor development induced by PTEN loss is mostly mediated by p110β. Further studies are needed to determine if this hypertrophic effect is mediated by p110α. It is possible that deletion of both p110α and p110β is needed to reverse the muscle size gain in m-PTEN$^{-/-}$ mice.

In summary, results presented in this chapter and in the previous chapter taken together suggest that downregulation of single PI3K isoforms, p110α or p110β has relatively minor effects on heart or skeletal muscle function and mass. However, when both PI3Ks are downregulated concurrently, the cardiac effects could be catastrophic. This could have important implications for the use of PI3K inhibitors in cancer patients.

Isoform-specific PI3K inhibitors will probably be better tolerated and have a higher therapeutic index as anti-cancer drugs than non-selective PI3K inhibitors.

Chapter 4

Differential Roles of p110α and p110β in Kras-Induced Pancreatic Tumorigenesis

4-1 Introduction

As discussed in Chapter 1, PI3K p110α and p110β are involved in tumorigenesis[17, 56, 71, 125-126]. Many genetic defects found in human cancers lead to upregulated PI3K signaling[2]. Activating mutations in the p110α gene have been identified in several human cancers[67, 127] and recent experiments in mice have shown that interaction between p110α and Kras is required for oncogenic Kras to induce lung tumors[125]. Many human cancers also exhibit loss of the tumor suppressor PTEN[40]. In contrast to Kras-induced lung tumorigenesis, prostate tumorigenesis induced by loss of PTEN as well as mammary tumorigenesis induced by ERB2 activation are p110β dependent[56, 71]. Currently, it is not clear whether the differential roles of p110 isoforms are due to tissue specificity or related to specific oncogene and tumor suppressor pathways. Whichever the case, these studies emphasize that targeting PI3K could be through either the use of broad spectrum inhibitors, which is likely to have more significant side effects, or by obtaining sufficient information about individual tumor types to target the appropriate p110 subunit specifically. With this in mind, studies in this chapter examined the contributions of PI3K isoforms to pancreatic tumorigenesis.

Pancreatic ductal adenocarcinoma (PDA) is the most common pancreatic cancer and has one of the lowest cancer survival rates in part due to its resistance to most chemotherapies. Greater than 90% of PDA is initiated by oncogenic mutation of the small

GTPase Kras. Although mechanisms of initiation and progression of lung, prostate and mammary gland tumor types in humans are widely heterogeneous, oncogenic mutations in Kras are found at all stages of pancreatic tumor progression[128].

In collaboration with Dr. Howard Crawford, I used a well-established animal model of PDA. The LSL-Kras^{G12D};Ptf1a-Cre PDA mouse[129], which harbors an oncogenic Kras allele whose expression is activated by Cre recombinase specifically targeted to the pancreas, closely mimics human PDA genetically and histopathologically[130]. This chapter describes the results from studies in which p110α or p110β was ablated in this Kras-induced PDA mouse model.

4-2 Materials and Methods

General Materials

Antibodies were purchased from commercial sources: p110α from BD Biosciences; Kras, p110β and Akt from Santa Cruz Biotechnology; pan-p85 and GSK3β from Millipore; and phospho-T308-Akt, phospho-S473-Akt, phospho-4E-BP1, 4E-BP1 and phospho-GSK3β from Cell Signaling. Western blot signals were visualized using horseradish peroxidase-linked secondary antibodies (Amersham Biosciences) and chemiluminescence reagents (PerkinElmer Life Sciences).

Animal Models

All animal-related experimental protocols were approved by the Stony Brook University Institutional Animal Care and Use Committee. In this chapter, we used two breeding programs between either heterozygous floxed p110α or heterozygous floxed

p110β mice and LSL-Kras^{G12D} and Ptf1a-Cre mice[130] to obtain p110α$^{Flox/Flox}$;Ptf1a-Cre, p110α$^{Flox/Flox}$;Kras^{G12D};Ptf1a-Cre, and p110α$^{WT/WT}$;Kras^{G12D};Ptf1a-Cre littermates and p110β$^{Flox/Flox}$;Ptf1a-Cre, p110β$^{Flox/Flox}$;Kras^{G12D};Ptf1a-Cre and p110β$^{WT/WT}$;Kras^{G12D};Ptf1a-Cre littermates. To obtain sufficient animals for these studies 6 mating pairs were maintained, having a minimum of 8 litters each. Mice of identical genotypes from distinct litters were indistinguishable from one another at all stages of analysis. Mice that carry p110$^{WT/WT}$ without Kras^{G12D} or mice that do not express Ptfla-Cre from either breeding program were used as controls in their respective groups. All genetically modified mice are in a mixed C57BL/6 and 129 genetic background. Phenotypic comparisons were made between knockout mouse strains and their respective p110-intact littermates.

Phosphopeptide Pull-Down of PI3K

PI3K pull-downs and western blotting were performed as previously described[65].

Activated Kras Assay

The Ras-binding domain (RBD) of human cRaf (a.a. 1-149) was subcloned into pGEX-5x-3 (GE Healthcare) and transformed into BL21 bacteria. The bacteria were grown at 37˚C until the OD_{600} reached 0.8 and then induced with 0.2 mM IPTG at 30˚C for 3.5 hr. The bacteria were harvested, suspended in buffer (20 mM Tris-HCl, pH 8.0, 500 mM NaCl, 1% Triton-100, 1 mM EDTA and protease inhibitors) and lysed in a French press. The resulting homogenate was clarified by centrifugation and mixed with Glutathione Sepharose 4B beads (GE Healthcare). The beads were washed with buffer (20 mM Tris-HCl, pH 8.0, 20% glycerol, 50 mM NaCl, 1 mM EDTA, and 1 mM DTT). Pancreas lysates in MLB buffer (25 mM Hepes, pH 7.5, 150 mM NaCl, 10 mM $MgCl_2$, 1 mM EDTA, 1% NP-40 and 10% glycerol) were mixed with GST-Raf-RBD beads and the

bound proteins were analyzed by western blotting with the Kras antibody.

Immunohistochemistry

Immunohistochemical analysis with the phospho-T308-Akt antibody (Epitomics, Burlingame, CA) on pancreatic sections was performed as previously described[131].

Activated Rac1 Assay

The p21-binding domain (PBD) of human PAK1 (a.a. 70-117) in pGEX2TK vector in BL21 bacterial was purchased from Addgene. The bacteria were grown at 37˚C until the OD_{600} reached 0.7~0.8 and then induced with 0.1 mM IPTG at 30˚C for 2.5 hr. The bacteria were harvested, suspended in buffer (50 mM Tris-HCl, pH 7.5, 150 mM NaCl, 1% Triton-100, 5 mM $MgCl_2$, 1 mM DTT and protease inhibitors) and lysed in a French press. The resulting homogenate was clarified by centrifugation and mixed with Glutathione Sepharose 4B beads (GE Healthcare). The beads were washed with buffer (50 mM Tris-HCl, pH 7.5, 10% glycerol, 150 mM NaCl, 0.5% Triton-100, 1 mM DTT and 0.1 mM PMSF). Pancreas lysates in MLB buffer were mixed with GST-PAK1-PBD beads and the bound proteins were analyzed by western blotting with the Rac1 antibody.

4-3 Results

4-3-1 Phenotypic Changes of Pancreas p110α-Null and p110β-Null Mice

To address if p110α or p110β plays a role in Kras-driven pancreatic tumorigenesis, we bred $p110\alpha^{Flox/Flox}$ or $p110\beta^{Flox/Flox}$ mice to the LSL-$Kras^{G12D}$ and Ptf1a-Cre mice, resulting in activation of $Kras^{G12D}$ expression and deletion of p110 in the same cells. Western blot analysis of pancreatic extracts showed that p110α protein was specifically

depleted in the p110α$^{-/-}$ pancreas (abbreviated as p-α$^{-/-}$ hereafter) as compared to the p110α$^{+/+}$ control (abbreviated as p-α$^{+/+}$ hereafter); conversely, p110β protein was specifically lost in the p110β$^{-/-}$ pancreas (abbreviated as p-β$^{-/-}$ hereafter) as compared to the p110β$^{+/+}$ control (abbreviated as p-β$^{+/+}$ hereafter) (Fig. 4-1).

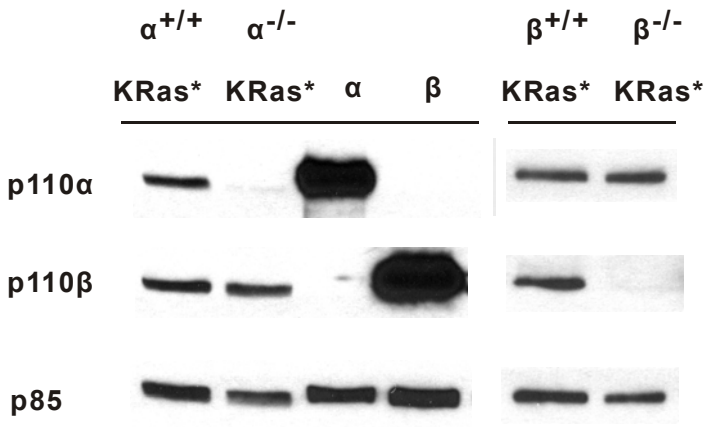

Fig. 4-1 Pancreas PI3K expression. Class IA PI3Ks in pancreas extracts were pulled down with a phosphotyrosine peptide coupled to agarose and then analyzed by western blotting with antibodies against p110α, p110β, or p85. Recombinant proteins p110α/p85α (α) and p110β/p85α (β) were loaded as controls. KRas* stands for mice expressing the oncogenic Kras^{G12D} mutant.

Mice lacking p110α or p110β in the pancreas were viable and fertile. The organs appeared normal (Fig. 4-2a), although the pancreata of p110α-null mice were consistently smaller, a phenotype that correlated to an overall smaller cell size (data not shown).

At 6 weeks of age, pancreata of LSL-Kras^{G12D};Ptf1a-Cre (abbreviated as KRas* hereafter) mice start to develop tumors, marked by focal pancreatic intraepithelial neoplasia (PanIN) and metaplastic and desmoplastic reaction throughout the pancreas[129]. KRas* mice showed multiple tumor lesions at 8 weeks of age, each displaying multiple

PanIN and metaplastic structures (Fig. 4-2a, c). Tumorigenesis in 8 week old mice resulted in a reproducible increase in the pancreatic wet weight/body weight ratio as compared to control (Fig. 4-2). When p110α was ablated in the KRas* mice, no increase in pancreatic mass was observed (Fig. 4-2b). Correspondingly, no tumors were found by gross or histological examination at 8 weeks of age (Fig. 4-2c). At 16 weeks of age, 2 of 6 p-$\alpha^{-/-}$;KRas* mice showed a single PanIN-like glandular structure with no desmoplastic reaction in the entirety of the pancreas. Examination of three 7 month old and two 12 month old p-$\alpha^{-/-}$;KRas* mice also showed no tumor formation, suggesting that the lack of tumors in younger mice is not due to a delay in onset, but to a long term blockade in tumor initiation. In contrast to p110α, pancreatic mass increased significantly and tumors formed efficiently in the KRas* mice when p110β was deleted (Fig. 4-2b, c). We conclude that p110α is specifically required for pancreatic tumor formation in the LSL-$Kras^{G12D}$;Ptf1a-Cre model of PDA.

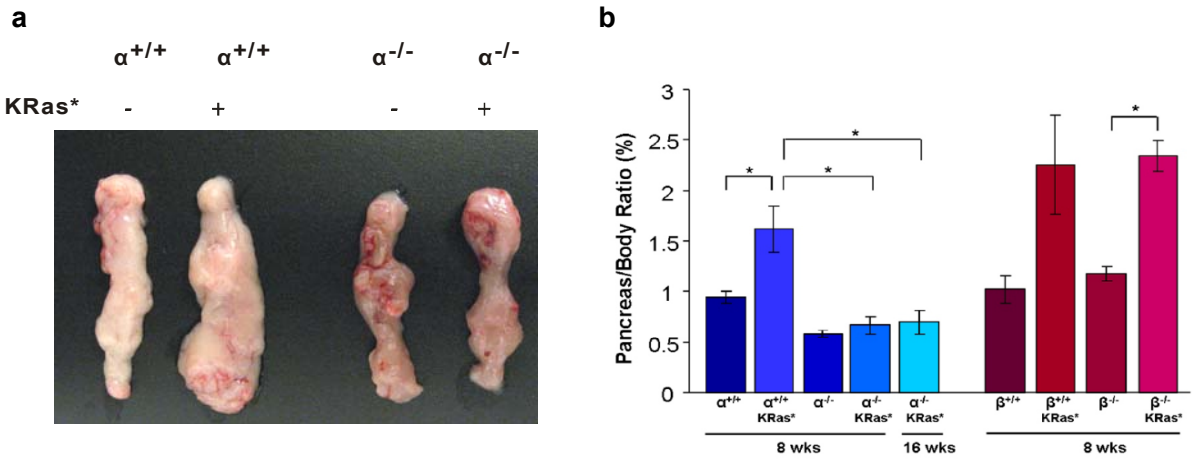

c

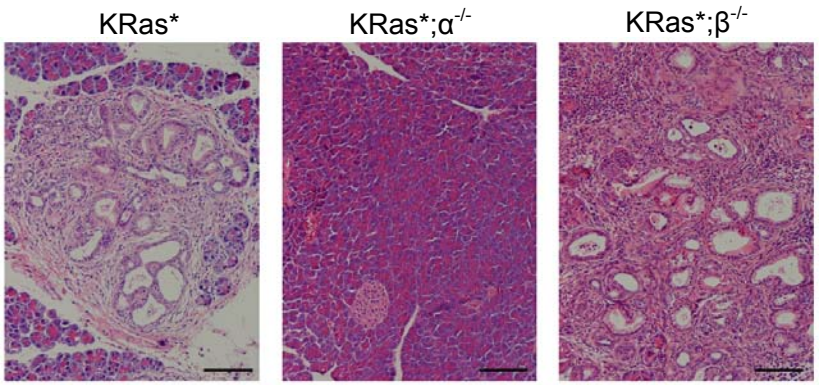

Fig. 4-2 Ablation of p110α blocks pancreatic tumor formation by oncogenic Kras. (**a**) Photograph of pancreata from 8 week old p-$\alpha^{+/+}$, p-$\alpha^{+/+}$;KRas*, p-$\alpha^{-/-}$, and p-$\alpha^{-/-}$;KRas* mice. (**b**) Pancreas wet weight/body weight ratios of 8 or 16 week old mice with the indicated genotypes (N = 6 per group, except N = 5 for p-$\alpha^{-/-}$;KRas*). Asterisks indicate P<0.01, ANOVA with post hoc Tukey test. (**c**) H&E staining of pancreas sections from mice of the indicated genotypes (scale bar = 100 μm).

4-3-2 Signaling in the Pancreas of p-$\alpha^{-/-}$;KRas* and p-$\beta^{-/-}$;KRas* Mice

To ensure that the lack of tumor formation in p-$\alpha^{-/-}$;KRas* pancreata was not due to downregulation of Kras protein expression, the immobilized Ras-binding domain of Raf (Raf-RBD) was used to pull down GTP-loaded Kras from pancreas lysates. Western blotting showed that the KRas* and p-$\alpha^{-/-}$;KRas* samples contained equivalent amounts of active Kras protein (Fig. 4-3).

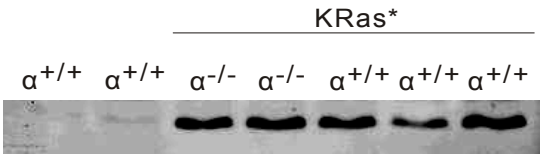

Fig. 4-3 Activated Ras proteins in pancreas extracts of the indicated genotypes were pulled down with immobilized Raf-RBD protein and then analyzed by western blotting with a Kras antibody.

We also used western blotting to examine the activation state of Akt, which is the

best known downstream signaling effector of PI3K. Previous studies have shown that activated Akt correlates with advanced progression and poor prognosis of PDA[132]. Unexpectedly, we observed an increase in phospho-Akt levels in p-$\alpha^{-/-}$ pancreata (with or without KRas*) as compared to control samples (with or without KRas*) (Fig. 4-4a), which was not observed in p-$\beta^{-/-}$ (with or without KRas*) samples. Similar changes in phosphorylation were observed in effectors downstream of Akt (Fig. 4-4a) in p-$\alpha^{-/-}$ pancreata (with or without KRas*), but not in p-$\beta^{-/-}$ (with or without KRas*) samples. To address the source of this increase in phospho-Akt, we performed immunohistochemistry using a phospho-T308-Akt antibody. In Kras* mice we found staining in tumor and metaplastic ductal epithelia as well as in normal intercalated ducts, but little to no staining in acinar cells (Fig. 4-4b). In contrast, p-$\alpha^{-/-}$;KRas* pancreata showed strong staining in both normal ducts and in the majority of acinar cells (Fig. 4-4b). Given that the bulk of the pancreas is made up of acinar cells, it is likely that the upregulation of phospho-Akt in acinar cells is the explanation for the overall higher levels of phospho-Akt in tissue lysates. Immunofluorescence studies using a phospho-S473-Akt antibody showed similar results (Fig. 4-4c). One possible explanation for this seemingly paradoxical increase in Akt activation in a p110α-null tissue is that ablation of p110α downregulates PTEN activity and thus leads to a higher level of phospho-Akt. Hyperactivation of Akt was also observed in p85α knockout liver, where there was a concomitant 70% decrease in p110α expression[133]. These investigators found that PTEN activity was reduced in the p85$\alpha^{-/-}$ liver without a change in protein expression[133]. We also did not detect a difference in PTEN protein level between KRas* and p-$\alpha^{-/-}$;KRas* pancreata (Fig. 4-4d). A second possibility is that there is increased recruitment of other PI3K isoforms to activated Kras in p-$\alpha^{-/-}$ acinar cells that results in increased Akt activity. In either case, activation of Akt in

the absence of p110α does not contribute to the formation of ductal tumors.

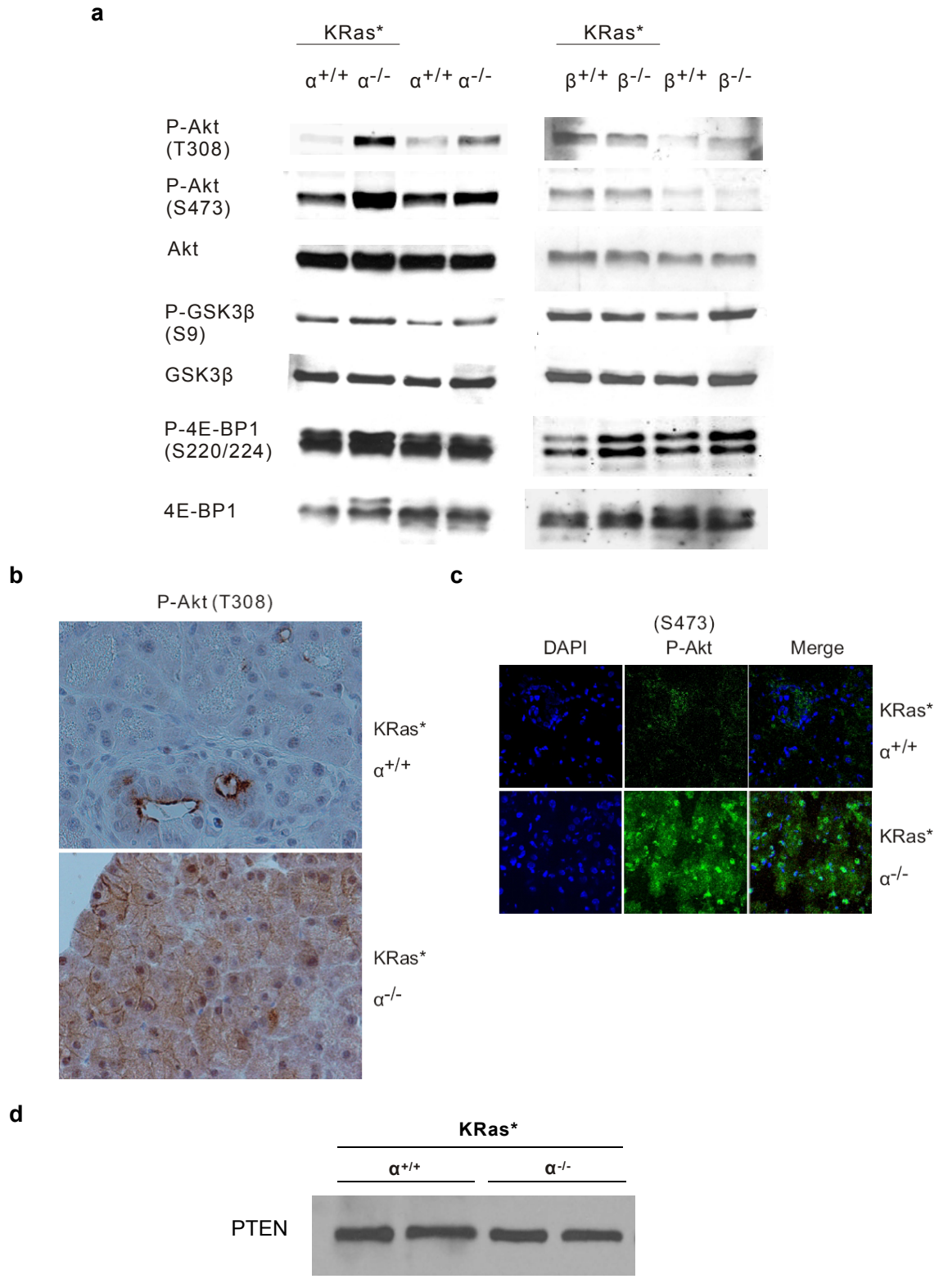

Fig. 4-4 Effect of Kras^{G12D} expression and PI3K knockout on cell signaling in pancreata. (**a**) Pancreas extracts were analyzed by western blotting with the indicated antibodies. (**b**) Immunohistochemical analysis was performed on pancreas sections using a phospho-T308-Akt antibody. (**c**) Immunofluorescence analysis was performed on pancreas sections using a phospho-S473-Akt antibody (green). The slides were counterstained with DAPI (blue) to reveal the nuclei. (**d**) Pancreas extracts were analyzed by western blotting with PTEN antibody.

As mentioned in Chapter 1, another downstream effector of PI3K is the GTPase Rac1. This protein has been reported to play an important role in regulating multiple signaling pathways that control cytoskeleton organization, transcription, and cell proliferation[134]. In addition, activated Rac1 is necessary for transformation and tumorigenesis induced by oncogenes including Ras[135-137]. Recent studies indicate that PI3K signaling to Rac1 is essential for Rac1 functions[138-139]. We therefore examined if KRas* pancreata have increased Rac1 activation and if ablation of p110α blocks this activation. GTP-loaded Rac1 was pulled down from p-α$^{+/+}$ or p-α$^{-/-}$ (with or without KRas*) pancreatic lysates using a recombinant p21-binding domain of PAK1 (PAK1-PBD) protein and then detected by western blotting. I found that p-α$^{+/+}$;KRas* pancreata had approximately 2.7 times more activated Rac1 than p-α$^{+/+}$ samples (Fig. 4-5). Importantly, the level of activated Rac1 in p-α$^{-/-}$;KRas* pancreata was much reduced as compared to p-α$^{+/+}$;KRas* tissue (Fig. 4-5). In addition, total Rac1 protein was increased 3.1-fold in lysates of p-α$^{+/+}$;KRas* pancreata as compared with p-α$^{+/+}$ samples, and this increase was also suppressed in the p-α$^{-/-}$;KRas* pancreata (Fig. 4-5). The level of activated Rac1 also increased more in p-β$^{+/+}$;KRas* samples than in p-β$^{-/-}$;KRas* pancreata as compared to p-β$^{+/+}$ (Fig. 4-5). However, unlike in the p-α$^{-/-}$;KRas* mice, the total amount of Rac1 was increased even more in the p-β$^{-/-}$;KRas* lysates than in the p-β$^{+/+}$;KRas* samples (Fig. 4-5). In conclusion, these results indicate that ablation of p110α, but not p110β, blocks the

increased expression and activation of Rac1 induced by oncogenic Kras. Further studies are needed to determine if Kras signaling through p110α to activate Rac1 is the mechanism responsible for the development of pancreatic tumors.

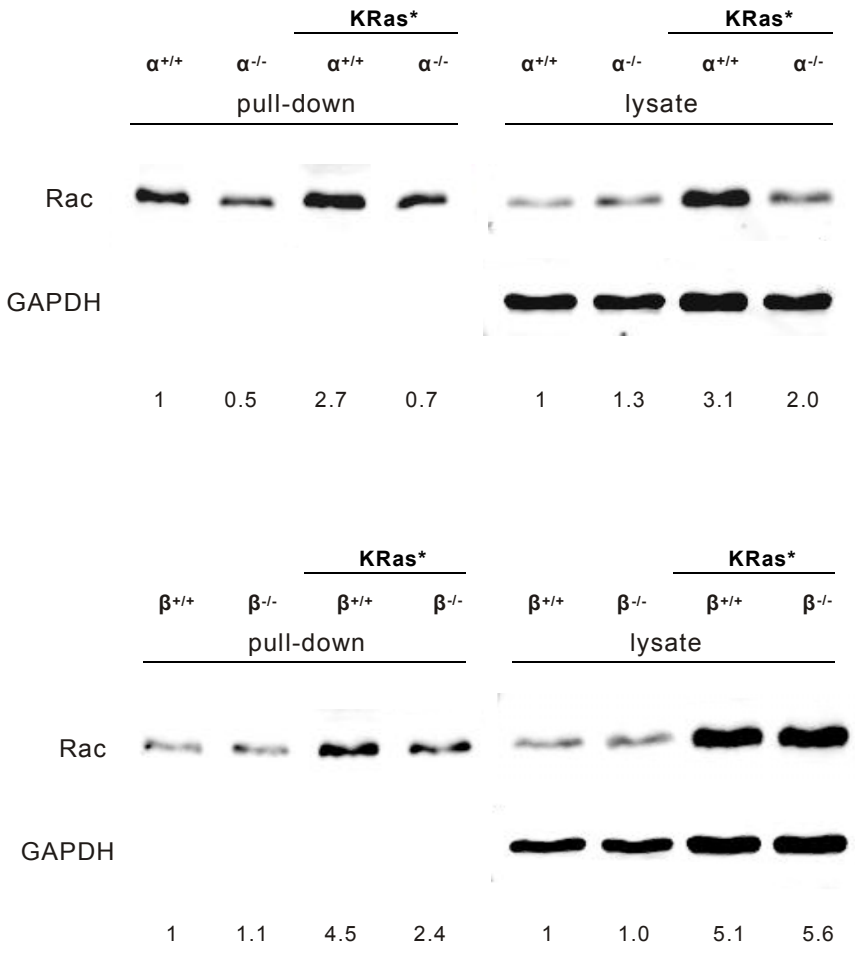

Fig. 4-5 Left panels: activated Rac proteins in pancreas lysates of the indicated genotypes were pulled down with immobilized PAK1-PBD protein and then analyzed by western blotting with a Rac1 antibody. Numbers under the lanes show quantification of the Rac1 bands. Values were normalized to signals for $\alpha^{+/+}$ or $\beta^{+/+}$. Right panels: total pancreas lysates were analyzed by western blotting with a Rac1 antibody. Numbers under the lanes show quantification of the Rac1/GAPDH ratios normalized to the values for $\alpha^{+/+}$ or $\beta^{+/+}$.

4-4 Discussion

Results from this study show that ablation of p110α, but not p110β, successfully blocks pancreatic tumor formation induced by oncogenic Kras. This inhibition is not due to downregulation of Kras activation or expression (expression data now shown). Neither is the inhibition of tumorigenesis due to decreased Akt activation. In fact, Akt is more activate in the $p110\alpha^{-/-}$;$KRas^{*}$ pancreas than the $KRas^{*}$ tissue. Our data suggested that another PI3K effector, Rac1, might be involved in p110α-dependent tumor formation because Rac1 is more activate in the $KRas^{*}$ pancreas than the $p110\alpha^{-/-}$;$KRas^{*}$ pancreas. In contrast, Rac1 activation was not lower in the $p110\beta^{-/-}$;$KRas^{*}$ pancreas than in the $KRas^{*}$ tissue. Future studies will investigate if Kras-induced tumorigenesis is also blocked in a Rac1-null pancreas. We also plan to determine if constitutively activate p110α or Rac1 will induce pancreatic tumors.

To better mimic the human condition, our future plans are to generate genetically modified mice that allow conditional deletion of p110α in the pancreas of $KRas^{*}$ mice. These models will better resemble pharmacological inhibition of p110α in established pancreatic tumors. Finally, there are a number of PI3K inhibitors already being tested in early phase clinical trials as anti-cancer drugs. These compounds can be tested in the $KRas^{*}$ mice to determine their efficacy against pancreatic cancer. Obviously, promising results from these experiments could lead to further testing in human trials for this deadly disease.

Chapter 5
Discussion and Future Studies

5-1 Discussion and future studies for Chapter 2

There are many unanswered questions from my studies in Chapter 2. The experiments described in this chapter are future studies that aim to further investigate how decreased PI3K signaling causes Ca^{2+}-handling abnormalities in cardiac myocytes. I hypothesize that PI3K p110α and p110β are required to maintain a normal T-tubule network and cardiac dyad structures needed to sustain excitation-contraction coupling in myocytes. To test this hypothesis, I propose the following three experiments:

1. Define the time course of T-tubule formation, cardiac dyad structure formation and PI3K downregulation during mouse cardiac myocyte development. In rat neonatal myocytes, plasma membrane LTCCs and RyR in the SR colocalize around the cell periphery because the plasma membrane has not yet started to invaginate[140]. T-tubules only start to develop at around day 6 after birth in rats[140]. The time course for T-tubule network formation has not been determined in mice. It is also unclear when the Ca^{2+}-handling proteins that assemble in the cardiac dyads are expressed and how they are sequentially localized to the proper membrane areas. These are important factors for my work using MCK-Cre to knock out PI3K genes because this promoter turns on at embryonic day 13.5 and shows maximal activity at 19-21 days after birth. I only examined T-tubule structure in 35-37 day old PI3K dKO mice. It is possible that T-tubules formed earlier in these mice and then became disrupted in older animals as the PI3K proteins

disappeared. To test this idea, I will collect hearts from control, $\alpha^{-/-}$, $\beta^{-/-}$ and dKO mice at ages 1, 7, 14 and 21 days. Samples will be analyzed by the following procedures:

a) Isolated myocytes will be stained with Di-8-ANEPPS to visualize the T-tubule network;

b) Electron microscopy will be done on thin sections of left ventricle to examine cardiac dyad structures;

c) Confocal immunofluorescence microscopy will be used to visualize colocalization of the LTCC and RyR;

d) RNA and protein isolated from hearts will be analyzed by real-time RT-PCR and western blotting to examine the expression of Ca^{2+}-handling proteins, including $Ca_V1.2$, RyR, triadin, junctin and CSQ2; and

e) The expression levels of p110α and p110β will be determined in lysates of isolated myocytes. In addition to samples prepared from mice of the ages listed above, this experiment will also use material prepared from myocytes of mice at embryonic day 18 and 8-week old adult mice (except for the dKO animals that do not survive to adulthood).

2. Characterize cardiac myocyte-specific conditional dKO mice. I have generated a tamoxifen-inducible cardiac myocyte-specific conditional p110α/p110β double knockout mouse strain. I generated these mice by breeding $p110\alpha^{Flox/Flox}$;$p110\beta^{Flox/Flox}$ mice to animals expressing a tamoxifen-regulated Cre recombinase (MerCreMer) that is under the control of a cardiac myocyte-specific αMHC promoter. Adult and fetal mice expressing $p110\alpha^{Flox/Flox}$;$p110\beta^{Flox/Flox}$;MerCreMer have intact p110 genes until they or the pregnant mothers are administered tamoxifen to activate the MerCreMer protein. Tamoxifen will be administered by mixing it into the food.

I will use these animals to determine if deletion of both PI3Ks in adult mice (8 weeks

of age) disrupts the T-tubule network and downregulates the expression of Ca^{2+}-handling proteins as outlined in Experiment 1. I will also measure myocyte contractility and Ca^{2+} transients in myocytes isolated from these adult animals. In addition, I will use the offspring of drug-treated pregnant females to confirm that embryonic deletion of both PI3Ks leads to cardiac phenotypes that are the same as those exhibited by the $p110\alpha^{Flox/Flox}$;$p110\beta^{Flox/Flox}$;MCK-Cre mice that were described in Chapter 2. In these experiments, littermates that do not express MerCreMer will undergo the same tamoxifen regimen as the experimental group and will be used as controls.

Expected results for the first two experiments—For experiment 1, I anticipate that the T-tubule network and cardiac dyad structures will be well formed by 14 days of age in all four groups of myocytes, including the dKO group. These myocytes will also have similar levels of p110α and p110β proteins. I expect the T-tubule and cardiac dyad structures to be abnormal in the 21-day old dKO myocytes, and this would correspond to a loss of the PI3Ks. Normal organization should still be present in the other three groups at this age. These results would support my hypothesis that PI3K p110α and p110β are required to maintain a normal T-tubule network and cardiac dyad structures. On the other hand, it is possible that the dKO myocyte T-tubule network will be disorganized at all the time points examined. This result would suggest that the etiology of structural abnormalities is developmental in nature and that the T-tubule organization is never completely formed in the dKO myocytes. My hypothesis would also be supported if ablation of both PI3Ks in adult mice using the inducible MerCreMer causes similar T-tubule network disruption. However, if I do not observe structural changes in adult dKO myocytes then this would suggest that p110α and p110β are required during post-natal cardiac development to

form a normal T-tubule network and cardiac dyads.

I expect that the changes in expression levels of Ca^{2+}-handling proteins will closely correlate with T-tubule disruption in the dKO hearts. Therefore, the expression will be decreased in dKO hearts as compared to control hearts at time points when the T-tubule network is disorganized. However, if the expression changes occur before the structural changes, then this might indicate that the T-tubule network cannot form in the absence of at least one of these proteins.

3. Identify regulatory molecules downstream of PI3K that control the expression of Ca^{2+}-handling proteins. Since multiple Ca^{2+}-handling proteins were downregulated in the dKO hearts, I hypothesize that one or more transcription factors downstream of PI3K might be regulating the expression of these proteins. FOXO family members are possible candidates. To determine if the nuclear localization of FOXO proteins is increased in the dKO myocytes as compared to controls, western blotting of nuclear and cytoplasmic fractions will be done. Western blotting of whole-cell lysates can also be done using phospho-specific antibodies to determine if Akt-dependent phosphorylation is decreased in the dKO cells. A search for FOXO binding sites in the promoters of the genes for Ca^{2+}-handling proteins might also be informative.

In another approach, I will isolate myocytes from control, $\alpha^{-/-}$, $\beta^{-/-}$, and dKO mice (age will depend on results from Experiment 1) and then extract RNA from these cells. The RNA will be analyzed by genomic techniques, either microarrays[141] or serial analysis of gene expression (SAGE)[142-143], to screen for potential regulatory molecules that are either up or down regulated in the dKO myocytes. Once identified, real-time RT-PCR and western blotting will be performed to confirm the expression changes of these regulatory

molecules.

5-2 Discussion and future studies for Chapter 3

The main result from this chapter is that at 2 months of age, muscle-specific p110α$^{-/-}$ mice have smaller muscles whereas the muscle size of p110β$^{-/-}$ mice is not different from their wildtype controls. The modest decrease in muscle size in p110α$^{-/-}$ mice did not lead to obvious detriments even when these animals were subjected to the stress of hind-limb suspension. One conclusion that can be drawn from these results is that inhibition of PI3K in the skeletal muscle would be well tolerated. However, is it really true that treating patients with PI3K inhibitors would not have any unwanted skeletal muscle side effects? This conclusion was based on my findings from knockout mouse models in which the PI3K genes were deleted during embryonic development. It is possible that the phenotypes would be very different if the gene deletion occurred in adult animals using conditional knockout mouse models. For example, the floxed p110α and p110β mice could be bred to mice expressing a tamoxifen-regulated Cre recombinase under the control of a skeletal muscle actin promoter. Adult mice can be injected with tamoxifen to delete one or both PI3K genes followed by characterization of their muscle size using microCT scanning, histological analysis of myotube size and muscle weights.

My studies thus far have focused on the characterization of muscle size in the knockout mice. However, in one preliminary study, I did find that the p110α$^{-/-}$ mice have greatly reduced general activity. It is possible that the loss of either PI3K could affect muscle function, such as strength and endurance. Muscle strength could be investigated using both *ex vivo* and *in vivo* techniques. Isolated muscle strips can be mounted on an

apparatus (a single channel force transducer)[144] to measure how much the muscle contracts in response to electrical stimulation and how much force is generated against a given resistance for a period of time. *In vivo*, the muscle strength of the mice can be measured by the wire hang test. In this test, mice are hung with only the front legs on a wire and the latency to fall is measured. In addition, muscle endurance of these knockout mice can be tested by using a small animal treadmill. Mice can be trained to run on the treadmill with varying speeds and angles of incline. The time it takes for the mouse fall off the treadmill due to exhaustion can then be used as an estimate of muscle endurance. However, since the PI3K genes in my mice are also knocked out in the heart, the endurance phenotype could be due to a cardiac defect (Chapter 2 single knockout mice). To test this, $p110\alpha^{Flox/Flox}$ or $p110\beta^{Flox/Flox}$ mice can be bred to mice expressing a Cre recombinase under the control of a skeletal muscle actin promoter which specifically expresses in skeletal muscle. Muscle strength and endurance tests would then be done on these skeletal muscle-specific PI3K knockout animals.

It is possible that IGF-1 activation of PI3K signaling to regulate muscle size is not through the canonical downstream effector Akt. Investigating other known downstream effectors of PI3K might provide useful information. I have already determined that there was no difference in PKCζ activity in p110α knockout mice vs. controls (data not shown). Experiments can be done to examine if IGF-1 activation of small GTPases Rac1 or Cdc42 play a role in regulating muscle size. Assay of Rac1 activation is described in Chapter 4 Methods. On the other hand, inhibition of PI3K activation by other hormones or nutrients or by muscle contraction might explain the decreased muscle size in this knockout mouse strain. Future studies can be designed to investigate how these factors affect PI3K signaling in the muscle[114, 145-146] and if ablation of p110α can block their effects

on this signaling pathway.

The last part of this chapter investigated the role of p110α and p110β in mediating the increased muscle size exhibited by the $PTEN^{-/-}$ mice. My result (Fig. 3-8) suggested that the $PTEN^{-/-}$ muscle phenotype could be at least partially reversed by deletion of p110α instead of p110β. Additional studies with more animals plus examination of myotube size and measurement of S6 kinase activity are needed to confirm this promising preliminary result. Accumulating evidence suggests that phenotypes induced by the loss of PTEN are not always reversed by simultaneous ablation of p110β. This might depend on the expression level of p110α vs. p110β in each organ or the localization of these two isoforms of PI3K. To test this, co-immunostaining of these two proteins could determine their relative expression levels and where these two proteins are located in cells.

5-3 Discussion and future studies for Chapter 4

Even though previous studies have shown that the presence of activated Akt correlates with progression of pancreatic ductal adenocarcinoma, we unexpectedly found by three different techniques--western blotting, immunohistochemistry (IHC) and immunofluorescence--that the Akt phosphorylation level is higher in the $p110\alpha^{-/-}$ pancreata with oncogenic Kras than in control pancreata with oncogenic Kras. Two possible mechanisms that could cause upregulation of Akt were mentioned in the results section in Chapter 4: (1) ablation of p110α downregulates PTEN activity and (2) there is increased recruitment of other PI3K isoforms to active Kras in $p110\alpha^{-/-}$ acinar cells that results in increased Akt activity. Below I discuss two other possibilities that could explain

this unexpected finding.

There is always a concern that in comparing cell signaling between normal and tumorous tissues, the differences observed are due to differences in cell types and not to the specific genetic manipulation. The relevant cells of interest for my study are the progenitor cells that give rise to the pancreatic tumor cells in the Kras pancreata. Potentially, identification of cell surface markers that can identify these progenitor cells would allow us to perform western blot (after cell sorting), IHC or immunofluorescence analyses to compare phospho-Akt levels in these critical cells.

Another concern is that there are three isoforms of Akt. Phospho-Akt antibodies currently available recognize all three isoforms. It is possible that only one Akt isoform is responsible for Kras-induced tumorigenesis and the phosphorylation level of that particular isoform is low in the $KRas^{*}$;$p110\alpha^{-/-}$ pancreas cells. High phospho-Akt levels observed in $p110\alpha^{-/-}$ pancreata could be due to phosphorylation of other Akt isoforms not relevant to the tumorigenic process. For example, it is known that Akt1 regulates cell growth whereas Akt2 is involved in the control of cell metabolism. Development of isoform-specific phospho-Akt antibodies would allow us to test this hypothesis. In addition, breeding of p48-Cre;LSL-$Kras^{G12D}$ mice to isoform-specific Akt knockout mice could also be informative and demonstrate their involvement in pancreatic tumorigenesis.

On the other hand, it is also possible that activation of Akt is not involved in Kras-induced pancreatic tumorigenesis. PI3K activates a number of signaling molecules other than Akt. As I have shown in Chapter 4, Rac1 activation and expression were both upregulated in the $KRas^{*}$ pancreata and these increases were blocked in the $KRas^{*}$;$p110\alpha^{-/-}$ but not in the $KRas^{*}$;$p110\beta^{-/-}$ pancreata. These results suggest that Rac1 might play a role in Kras-induced pancreatic tumorigenesis. Future experiments using an

antibody that specifically recognizes activated Rac1 (GTP-bound) could help us determine the pancreatic cell types involved. To further test the role of Rac1 in tumorigenesis, p48-Cre;LSL-Kras^{G12D} mice could be bred to Rac1$^{flox/flox}$ mice (available from Jackson Laboratory) to generate Rac1 pancreatic knockouts in the Kras* background. In addition, KRas* mice could be treated with Rac1 inhibitors to investigate if pancreatic tumor formation is inhibited by the drug.

Interestingly, we found that p110α$^{-/-}$ pancreas cells are consistently smaller than controls. I wonder if PI3K regulation of cell size can play a role in tumor formation. It is well known that the mTOR/S6K signaling pathway, which is a downstream effector pathway of PI3K, is a critical regulator of cell size. Mice lacking S6K1 have smaller cells in most tissue types. p48-Cre;LSL-Kras^{G12D} mice could be bred to the S6K1$^{flox/flox}$ mice to see if the pancreas cells are smaller and if Kras-induced tumor formation is blocked.

The discussion above is based on the assumption that PI3K is a downstream catalytic effector of Kras. According to that assumption, Kras-induced tumor formation would also be blocked by genetic deletion of a downstream effector of p110α. However, an alternative possibility is that p110α is acting as a binding partner of Kras to target the G protein to a specific subcellular location that is required to induce oncogenesis. To investigate if p110α is acting in this scaffold protein-like manner, we could breed KRas*;α$^{-/-}$ mice to transgenic mice expressing a kinase-dead p110α mutant (p110α KD) in the pancreas. If this hypothesis is true then the p110α KD;KRas*;p110α$^{-/-}$ mice should develop pancreatic tumors.

General Conclusion

It has been more than 2 decades since PI3K was first discovered. The PI3K signaling pathway is a central node in the signal transduction system that regulates many essential cellular functions. Dysregulated PI3K signaling occurs frequently in human diseases. Therefore, PI3Ks have become promising targets for therapeutic intervention in immunological, metabolic and oncological disorders. A variety of studies have been done to better understand the diverse roles of PI3K signaling, including those aimed at dissecting the distinct biological roles of individual PI3K isoforms. However, there has been a concern that broad spectrum PI3K inhibitors might cause untoward side effects. My thesis work composed of three independent lines of research as described in Chapters 2-4 supports the validity of this concern. My research revealed that the two ubiquitous PI3K isoforms p110α and p110β play distinct biological roles in a tissue-specific manner. Inhibition of both PI3Ks appears to have very detrimental effects on heart function whereas inhibition of p110α alone potentially can block the development of pancreatic tumors. Furthermore, inhibition of single PI3K isoforms in the skeletal muscle seems to be very well tolerated. My thesis research supports the benefits of generating selective drugs that target specific PI3K isoforms. It is my sincere hope that this information will lead to the successful development of clinically useful PI3K inhibitors for the treatment of human diseases.

Reference

1. Stokoe D. The phosphoinositide 3-kinase pathway and cancer. *Expert Rev Mol Med*. 2005;7:1-22
2. Osaki M, Oshimura M, Ito H. Pi3k-akt pathway: Its functions and alterations in human cancer. *Apoptosis*. 2004;9:667-676
3. Wymann MP, Pirola L. Structure and function of phosphoinositide 3-kinases. *Biochim Biophys Acta*. 1998;1436:127-150
4. Auger KR, Serunian LA, Soltoff SP, Libby P, Cantley LC. Pdgf-dependent tyrosine phosphorylation stimulates production of novel polyphosphoinositides in intact cells. *Cell*. 1989;57:167-175
5. Whitman M, Kaplan DR, Schaffhausen B, Cantley L, Roberts TM. Association of phosphatidylinositol kinase activity with polyoma middle-t competent for transformation. *Nature*. 1985;315:239-242
6. Auger KR, Carpenter CL, Shoelson SE, Piwnica-Worms H, Cantley LC. Polyoma virus middle t antigen-pp60c-src complex associates with purified phosphatidylinositol 3-kinase in vitro. *J Biol Chem*. 1992;267:5408-5415
7. Ruderman NB, Kapeller R, White MF, Cantley LC. Activation of phosphatidylinositol 3-kinase by insulin. *Proc Natl Acad Sci U S A*. 1990;87:1411-1415
8. Escobedo JA, Navankasattusas S, Kavanaugh WM, Milfay D, Fried VA, Williams LT. Cdna cloning of a novel 85 kd protein that has sh2 domains and regulates binding of pi3-kinase to the pdgf beta-receptor. *Cell*. 1991;65:75-82
9. Skolnik EY, Margolis B, Mohammadi M, Lowenstein E, Fischer R, Drepps A, Ullrich A, Schlessinger J. Cloning of pi3 kinase-associated p85 utilizing a novel method for expression/cloning of target proteins for receptor tyrosine kinases. *Cell*. 1991;65:83-90
10. Otsu M, Hiles I, Gout I, Fry MJ, Ruiz-Larrea F, Panayotou G, Thompson A, Dhand R, Hsuan J, Totty N, et al. Characterization of two 85 kd proteins that associate with receptor tyrosine kinases, middle-t/pp60c-src complexes, and pi3-kinase. *Cell*. 1991;65:91-104
11. Gout I, Dhand R, Panayotou G, Fry MJ, Hiles I, Otsu M, Waterfield MD. Expression and characterization of the p85 subunit of the phosphatidylinositol 3-kinase complex and a related p85 beta protein by using the baculovirus

expression system. *Biochem J*. 1992;288 (Pt 2):395-405

12. Hu P, Mondino A, Skolnik EY, Schlessinger J. Cloning of a novel, ubiquitously expressed human phosphatidylinositol 3-kinase and identification of its binding site on p85. *Mol Cell Biol*. 1993;13:7677-7688
13. Vanhaesebroeck B, Waterfield MD. Signaling by distinct classes of phosphoinositide 3-kinases. *Exp Cell Res*. 1999;253:239-254
14. Wymann MP, Zvelebil M, Laffargue M. Phosphoinositide 3-kinase signalling--which way to target? *Trends Pharmacol Sci*. 2003;24:366-376
15. Wu H, Yan Y, Backer JM. Regulation of class ia pi3ks. *Biochem Soc Trans*. 2007;35:242-244
16. Samuels Y, Ericson K. Oncogenic pi3k and its role in cancer. *Curr Opin Oncol*. 2006;18:77-82
17. Vogt PK, Kang S, Elsliger MA, Gymnopoulos M. Cancer-specific mutations in phosphatidylinositol 3-kinase. *Trends Biochem Sci*. 2007;32:342-349
18. Foukas LC, Claret M, Pearce W, Okkenhaug K, Meek S, Peskett E, Sancho S, Smith AJ, Withers DJ, Vanhaesebroeck B. Critical role for the p110alpha phosphoinositide-3-oh kinase in growth and metabolic regulation. *Nature*. 2006;441:366-370
19. Sasaki T, Irie-Sasaki J, Jones RG, Oliveira-dos-Santos AJ, Stanford WL, Bolon B, Wakeham A, Itie A, Bouchard D, Kozieradzki I, Joza N, Mak TW, Ohashi PS, Suzuki A, Penninger JM. Function of pi3kgamma in thymocyte development, t cell activation, and neutrophil migration. *Science*. 2000;287:1040-1046
20. Hirsch E, Katanaev VL, Garlanda C, Azzolino O, Pirola L, Silengo L, Sozzani S, Mantovani A, Altruda F, Wymann MP. Central role for g protein-coupled phosphoinositide 3-kinase gamma in inflammation. *Science*. 2000;287:1049-1053
21. Barberis L, Hirsch E. Targeting phosphoinositide 3-kinase gamma to fight inflammation and more. *Thromb Haemost*. 2008;99:279-285
22. Crackower MA, Oudit GY, Kozieradzki I, Sarao R, Sun H, Sasaki T, Hirsch E, Suzuki A, Shioi T, Irie-Sasaki J, Sah R, Cheng HY, Rybin VO, Lembo G, Fratta L, Oliveira-dos-Santos AJ, Benovic JL, Kahn CR, Izumo S, Steinberg SF, Wymann MP, Backx PH, Penninger JM. Regulation of myocardial contractility and cell size by distinct pi3k-pten signaling pathways. *Cell*. 2002;110:737-749
23. Falasca M, Maffucci T. Role of class ii phosphoinositide 3-kinase in cell signalling. *Biochem Soc Trans*. 2007;35:211-214
24. Falasca M, Hughes WE, Dominguez V, Sala G, Fostira F, Fang MQ, Cazzolli R, Shepherd PR, James DE, Maffucci T. The role of phosphoinositide 3-kinase

c2alpha in insulin signaling. *J Biol Chem*. 2007;282:28226-28236

25. Elis W, Triantafellow E, Wolters NM, Sian KR, Caponigro G, Borawski J, Gaither LA, Murphy LO, Finan PM, Mackeigan JP. Down-regulation of class ii phosphoinositide 3-kinase alpha expression below a critical threshold induces apoptotic cell death. *Mol Cancer Res*. 2008;6:614-623
26. Ng SK, Neo SY, Yap YW, Karuturi RK, Loh ES, Liau KH, Ren EC. Ablation of phosphoinositide-3-kinase class ii alpha suppresses hepatoma cell proliferation. *Biochem Biophys Res Commun*. 2009;387:310-315
27. Backer JM. The regulation and function of class iii pi3ks: Novel roles for vps34. *Biochem J*. 2008;410:1-17
28. Kihara A, Noda T, Ishihara N, Ohsumi Y. Two distinct vps34 phosphatidylinositol 3-kinase complexes function in autophagy and carboxypeptidase y sorting in saccharomyces cerevisiae. *J Cell Biol*. 2001;152:519-530
29. Nobukuni T, Joaquin M, Roccio M, Dann SG, Kim SY, Gulati P, Byfield MP, Backer JM, Natt F, Bos JL, Zwartkruis FJ, Thomas G. Amino acids mediate mtor/raptor signaling through activation of class 3 phosphatidylinositol 3oh-kinase. *Proc Natl Acad Sci U S A*. 2005;102:14238-14243
30. Hawkins PT, Anderson KE, Davidson K, Stephens LR. Signalling through class i pi3ks in mammalian cells. *Biochem Soc Trans*. 2006;34:647-662
31. Marone R, Cmiljanovic V, Giese B, Wymann MP. Targeting phosphoinositide 3-kinase: Moving towards therapy. *Biochim Biophys Acta*. 2008;1784:159-185
32. Guillermet-Guibert J, Bjorklof K, Salpekar A, Gonella C, Ramadani F, Bilancio A, Meek S, Smith AJ, Okkenhaug K, Vanhaesebroeck B. The p110beta isoform of phosphoinositide 3-kinase signals downstream of g protein-coupled receptors and is functionally redundant with p110gamma. *Proc Natl Acad Sci U S A*. 2008;105:8292-8297
33. Rodriguez-Viciana P, Warne PH, Dhand R, Vanhaesebroeck B, Gout I, Fry MJ, Waterfield MD, Downward J. Phosphatidylinositol-3-oh kinase as a direct target of ras. *Nature*. 1994;370:527-532
34. Rodriguez-Viciana P, Sabatier C, McCormick F. Signaling specificity by ras family gtpases is determined by the full spectrum of effectors they regulate. *Mol Cell Biol*. 2004;24:4943-4954
35. Leslie NR, Downes CP. Pten: The down side of pi 3-kinase signalling. *Cell Signal*. 2002;14:285-295
36. Carracedo A, Pandolfi PP. The pten-pi3k pathway: Of feedbacks and cross-talks. *Oncogene*. 2008;27:5527-5541

37. Gericke A, Munson M, Ross AH. Regulation of the pten phosphatase. *Gene*. 2006;374:1-9
38. Stambolic V, Suzuki A, de la Pompa JL, Brothers GM, Mirtsos C, Sasaki T, Ruland J, Penninger JM, Siderovski DP, Mak TW. Negative regulation of pkb/akt-dependent cell survival by the tumor suppressor pten. *Cell*. 1998;95:29-39
39. Sun H, Lesche R, Li DM, Liliental J, Zhang H, Gao J, Gavrilova N, Mueller B, Liu X, Wu H. Pten modulates cell cycle progression and cell survival by regulating phosphatidylinositol 3,4,5,-trisphosphate and akt/protein kinase b signaling pathway. *Proc Natl Acad Sci U S A*. 1999;96:6199-6204
40. Jiang BH, Liu LZ. Pi3k/pten signaling in tumorigenesis and angiogenesis. *Biochim Biophys Acta*. 2008;1784:150-158
41. Keniry M, Parsons R. The role of pten signaling perturbations in cancer and in targeted therapy. *Oncogene*. 2008;27:5477-5485
42. Sarbassov DD, Guertin DA, Ali SM, Sabatini DM. Phosphorylation and regulation of akt/pkb by the rictor-mtor complex. *Science*. 2005;307:1098-1101
43. Brunet A, Bonni A, Zigmond MJ, Lin MZ, Juo P, Hu LS, Anderson MJ, Arden KC, Blenis J, Greenberg ME. Akt promotes cell survival by phosphorylating and inhibiting a forkhead transcription factor. *Cell*. 1999;96:857-868
44. Pap M, Cooper GM. Role of glycogen synthase kinase-3 in the phosphatidylinositol 3-kinase/akt cell survival pathway. *J Biol Chem*. 1998;273:19929-19932
45. Manning BD, Cantley LC. Akt/pkb signaling: Navigating downstream. *Cell*. 2007;129:1261-1274
46. Guertin DA, Sabatini DM. Defining the role of mtor in cancer. *Cancer Cell*. 2007;12:9-22
47. Yang Q, Guan KL. Expanding mtor signaling. *Cell Res*. 2007;17:666-681
48. Guertin DA, Stevens DM, Thoreen CC, Burds AA, Kalaany NY, Moffat J, Brown M, Fitzgerald KJ, Sabatini DM. Ablation in mice of the mtorc components raptor, rictor, or mlst8 reveals that mtorc2 is required for signaling to akt-foxo and pkcalpha, but not s6k1. *Dev Cell*. 2006;11:859-871
49. Schmidt A, Hall A. Guanine nucleotide exchange factors for rho gtpases: Turning on the switch. *Genes Dev*. 2002;16:1587-1609
50. Bernards A, Settleman J. Gap control: Regulating the regulators of small gtpases. *Trends Cell Biol*. 2004;14:377-385
51. Hawkins PT, Eguinoa A, Qiu RG, Stokoe D, Cooke FT, Walters R, Wennstrom S,

Claesson-Welsh L, Evans T, Symons M, et al. Pdgf stimulates an increase in gtp-rac via activation of phosphoinositide 3-kinase. *Curr Biol*. 1995;5:393-403

52. Krugmann S, Anderson KE, Ridley SH, Risso N, McGregor A, Coadwell J, Davidson K, Eguinoa A, Ellson CD, Lipp P, Manifava M, Ktistakis N, Painter G, Thuring JW, Cooper MA, Lim ZY, Holmes AB, Dove SK, Michell RH, Grewal A, Nazarian A, Erdjument-Bromage H, Tempst P, Stephens LR, Hawkins PT. Identification of arap3, a novel pi3k effector regulating both arf and rho gtpases, by selective capture on phosphoinositide affinity matrices. *Mol Cell*. 2002;9:95-108
53. Shioi T, Kang PM, Douglas PS, Hampe J, Yballe CM, Lawitts J, Cantley LC, Izumo S. The conserved phosphoinositide 3-kinase pathway determines heart size in mice. *EMBO J*. 2000;19:2537-2548
54. Shioi T, McMullen JR, Kang PM, Douglas PS, Obata T, Franke TF, Cantley LC, Izumo S. Akt/protein kinase b promotes organ growth in transgenic mice. *Mol Cell Biol*. 2002;22:2799-2809
55. Knobbe CB, Lapin V, Suzuki A, Mak TW. The roles of pten in development, physiology and tumorigenesis in mouse models: A tissue-by-tissue survey. *Oncogene*. 2008;27:5398-5415
56. Ciraolo E, Iezzi M, Marone R, Marengo S, Curcio C, Costa C, Azzolino O, Gonella C, Rubinetto C, Wu H, Dastru W, Martin EL, Silengo L, Altruda F, Turco E, Lanzetti L, Musiani P, Ruckle T, Rommel C, Backer JM, Forni G, Wymann MP, Hirsch E. Phosphoinositide 3-kinase p110{beta} activity: Key role in metabolism and mammary gland cancer but not development. *Sci Signal*. 2008;1:ra3
57. Chen WS, Xu PZ, Gottlob K, Chen ML, Sokol K, Shiyanova T, Roninson I, Weng W, Suzuki R, Tobe K, Kadowaki T, Hay N. Growth retardation and increased apoptosis in mice with homozygous disruption of the akt1 gene. *Genes Dev*. 2001;15:2203-2208
58. Peng XD, Xu PZ, Chen ML, Hahn-Windgassen A, Skeen J, Jacobs J, Sundararajan D, Chen WS, Crawford SE, Coleman KG, Hay N. Dwarfism, impaired skin development, skeletal muscle atrophy, delayed bone development, and impeded adipogenesis in mice lacking akt1 and akt2. *Genes Dev*. 2003;17:1352-1365
59. Richardson CJ, Schalm SS, Blenis J. Pi3-kinase and tor: Piktoring cell growth. *Semin Cell Dev Biol*. 2004;15:147-159
60. Bentzinger CF, Romanino K, Cloetta D, Lin S, Mascarenhas JB, Oliveri F, Xia J, Casanova E, Costa CF, Brink M, Zorzato F, Hall MN, Ruegg MA. Skeletal

muscle-specific ablation of raptor, but not of rictor, causes metabolic changes and results in muscle dystrophy. *Cell Metab*. 2008;8:411-424

61. Aguilar V, Alliouachene S, Sotiropoulos A, Sobering A, Athea Y, Djouadi F, Miraux S, Thiaudiere E, Foretz M, Viollet B, Diolez P, Bastin J, Benit P, Rustin P, Carling D, Sandri M, Ventura-Clapier R, Pende M. S6 kinase deletion suppresses muscle growth adaptations to nutrient availability by activating amp kinase. *Cell Metab*. 2007;5:476-487
62. Polak P, Hall MN. Mtor and the control of whole body metabolism. *Curr Opin Cell Biol*. 2009;21:209-218
63. Kerfant BG, Gidrewicz D, Sun H, Oudit GY, Penninger JM, Backx PH. Cardiac sarcoplasmic reticulum calcium release and load are enhanced by subcellular camp elevations in pi3kgamma-deficient mice. *Circ Res*. 2005;96:1079-1086
64. Sun H, Kerfant BG, Zhao D, Trivieri MG, Oudit GY, Penninger JM, Backx PH. Insulin-like growth factor-1 and pten deletion enhance cardiac l-type ca2+ currents via increased pi3kalpha/pkb signaling. *Circ Res*. 2006;98:1390-1397
65. Lu Z, Jiang YP, Wang W, Xu XH, Mathias RT, Entcheva E, Ballou LM, Cohen IS, Lin RZ. Loss of cardiac phosphoinositide 3-kinase p110 alpha results in contractile dysfunction. *Circulation*. 2009;120:318-325
66. Lu Z, Jiang YP, Xu XH, Ballou LM, Cohen IS, Lin RZ. Decreased l-type ca2+ current in cardiac myocytes of type 1 diabetic akita mice due to reduced phosphatidylinositol 3-kinase signaling. *Diabetes*. 2007;56:2780-2789
67. Samuels Y, Wang Z, Bardelli A, Silliman N, Ptak J, Szabo S, Yan H, Gazdar A, Powell SM, Riggins GJ, Willson JK, Markowitz S, Kinzler KW, Vogelstein B, Velculescu VE. High frequency of mutations of the pik3ca gene in human cancers. *Science*. 2004;304:554
68. Arcaro A, Guerreiro AS. The phosphoinositide 3-kinase pathway in human cancer: Genetic alterations and therapeutic implications. *Curr Genomics*. 2007;8:271-306
69. Engelman JA, Luo J, Cantley LC. The evolution of phosphatidylinositol 3-kinases as regulators of growth and metabolism. *Nat Rev Genet*. 2006;7:606-619
70. Wullschleger S, Loewith R, Hall MN. Tor signaling in growth and metabolism. *Cell*. 2006;124:471-484
71. Jia S, Liu Z, Zhang S, Liu P, Zhang L, Lee SH, Zhang J, Signoretti S, Loda M, Roberts TM, Zhao JJ. Essential roles of pi(3)k-p110beta in cell growth, metabolism and tumorigenesis. *Nature*. 2008;454:776-779
72. Asano T, Fujishiro M, Kushiyama A, Nakatsu Y, Yoneda M, Kamata H, Sakoda H. Role of phosphatidylinositol 3-kinase activation on insulin action and its

alteration in diabetic conditions. *Biol Pharm Bull*. 2007;30:1610-1616

73. Knight ZA, Gonzalez B, Feldman ME, Zunder ER, Goldenberg DD, Williams O, Loewith R, Stokoe D, Balla A, Toth B, Balla T, Weiss WA, Williams RL, Shokat KM. A pharmacological map of the pi3-k family defines a role for p110alpha in insulin signaling. *Cell*. 2006;125:733-747
74. Chaussade C, Rewcastle GW, Kendall JD, Denny WA, Cho K, Gronning LM, Chong ML, Anagnostou SH, Jackson SP, Daniele N, Shepherd PR. Evidence for functional redundancy of class ia pi3k isoforms in insulin signalling. *Biochem J*. 2007;404:449-458
75. Cho H, Mu J, Kim JK, Thorvaldsen JL, Chu Q, Crenshaw EB, 3rd, Kaestner KH, Bartolomei MS, Shulman GI, Birnbaum MJ. Insulin resistance and a diabetes mellitus-like syndrome in mice lacking the protein kinase akt2 (pkb beta). *Science*. 2001;292:1728-1731
76. Um SH, D'Alessio D, Thomas G. Nutrient overload, insulin resistance, and ribosomal protein s6 kinase 1, s6k1. *Cell Metab*. 2006;3:393-402
77. Um SH, Frigerio F, Watanabe M, Picard F, Joaquin M, Sticker M, Fumagalli S, Allegrini PR, Kozma SC, Auwerx J, Thomas G. Absence of s6k1 protects against age- and diet-induced obesity while enhancing insulin sensitivity. *Nature*. 2004;431:200-205
78. Cain RJ, Ridley AJ. Phosphoinositide 3-kinases in cell migration. *Biol Cell*. 2009;101:13-29
79. Graupera M, Guillermet-Guibert J, Foukas LC, Phng LK, Cain RJ, Salpekar A, Pearce W, Meek S, Millan J, Cutillas PR, Smith AJ, Ridley AJ, Ruhrberg C, Gerhardt H, Vanhaesebroeck B. Angiogenesis selectively requires the p110alpha isoform of pi3k to control endothelial cell migration. *Nature*. 2008;453:662-666
80. Yip SC, El-Sibai M, Coniglio SJ, Mouneimne G, Eddy RJ, Drees BE, Neilsen PO, Goswami S, Symons M, Condeelis JS, Backer JM. The distinct roles of ras and rac in pi 3-kinase-dependent protrusion during egf-stimulated cell migration. *J Cell Sci*. 2007;120:3138-3146
81. Orchard C, Brette F. T-tubules and sarcoplasmic reticulum function in cardiac ventricular myocytes. *Cardiovasc Res*. 2008;77:237-244
82. Brette F, Orchard C. Resurgence of cardiac t-tubule research. *Physiology (Bethesda)*. 2007;22:167-173
83. Franzini-Armstrong C. Architecture and regulation of the ca2+ delivery system in muscle cells. *Appl Physiol Nutr Metab*. 2009;34:323-327
84. Chopra N, Yang T, Asghari P, Moore ED, Huke S, Akin B, Cattolica RA, Perez CF,

Hlaing T, Knollmann-Ritschel BE, Jones LR, Pessah IN, Allen PD, Franzini-Armstrong C, Knollmann BC. Ablation of triadin causes loss of cardiac ca2+ release units, impaired excitation-contraction coupling, and cardiac arrhythmias. *Proc Natl Acad Sci U S A*. 2009;106:7636-7641

85. Yuan Q, Fan GC, Dong M, Altschafl B, Diwan A, Ren X, Hahn HH, Zhao W, Waggoner JR, Jones LR, Jones WK, Bers DM, Dorn GW, 2nd, Wang HS, Valdivia HH, Chu G, Kranias EG. Sarcoplasmic reticulum calcium overloading in junctin deficiency enhances cardiac contractility but increases ventricular automaticity. *Circulation*. 2007;115:300-309
86. Knollmann BC, Chopra N, Hlaing T, Akin B, Yang T, Ettensohn K, Knollmann BE, Horton KD, Weissman NJ, Holinstat I, Zhang W, Roden DM, Jones LR, Franzini-Armstrong C, Pfeifer K. Casq2 deletion causes sarcoplasmic reticulum volume increase, premature ca2+ release, and catecholaminergic polymorphic ventricular tachycardia. *J Clin Invest*. 2006;116:2510-2520
87. Takeshima H, Komazaki S, Nishi M, Iino M, Kangawa K. Junctophilins: A novel family of junctional membrane complex proteins. *Mol Cell*. 2000;6:11-22
88. Franzini-Armstrong C, Protasi F, Tijskens P. The assembly of calcium release units in cardiac muscle. *Ann N Y Acad Sci*. 2005;1047:76-85
89. Bi L, Okabe I, Bernard DJ, Wynshaw-Boris A, Nussbaum RL. Proliferative defect and embryonic lethality in mice homozygous for a deletion in the p110alpha subunit of phosphoinositide 3-kinase. *J Biol Chem*. 1999;274:10963-10968
90. Bi L, Okabe I, Bernard DJ, Nussbaum RL. Early embryonic lethality in mice deficient in the p110beta catalytic subunit of pi 3-kinase. *Mamm Genome*. 2002;13:169-172
91. Fan G, Jiang YP, Lu Z, Martin DW, Kelly DJ, Zuckerman JM, Ballou LM, Cohen IS, Lin RZ. A transgenic mouse model of heart failure using inducible galpha q. *J Biol Chem*. 2005;280:40337-40346
92. Costes SV, Daelemans D, Cho EH, Dobbin Z, Pavlakis G, Lockett S. Automatic and quantitative measurement of protein-protein colocalization in live cells. *Biophys J*. 2004;86:3993-4003
93. Rosati B, Dun W, Hirose M, Boyden PA, McKinnon D. Molecular basis of the t- and l-type ca2+ currents in canine purkinje fibres. *J Physiol*. 2007;579:465-471
94. Bruning JC, Michael MD, Winnay JN, Hayashi T, Horsch D, Accili D, Goodyear LJ, Kahn CR. A muscle-specific insulin receptor knockout exhibits features of the metabolic syndrome of niddm without altering glucose tolerance. *Mol Cell*. 1998;2:559-569

95. Hoyer K, Krenz M, Robbins J, Ingwall JS. Shifts in the myosin heavy chain isozymes in the mouse heart result in increased energy efficiency. *J Mol Cell Cardiol*. 2007;42:214-221
96. Bers DM. Cardiac excitation-contraction coupling. *Nature*. 2002;415:198-205
97. Takeshima H, Komazaki S, Hirose K, Nishi M, Noda T, Iino M. Embryonic lethality and abnormal cardiac myocytes in mice lacking ryanodine receptor type 2. *EMBO J*. 1998;17:3309-3316
98. Seisenberger C, Specht V, Welling A, Platzer J, Pfeifer A, Kuhbandner S, Striessnig J, Klugbauer N, Feil R, Hofmann F. Functional embryonic cardiomyocytes after disruption of the l-type alpha1c (cav1.2) calcium channel gene in the mouse. *J Biol Chem*. 2000;275:39193-39199
99. Periasamy M, Reed TD, Liu LH, Ji Y, Loukianov E, Paul RJ, Nieman ML, Riddle T, Duffy JJ, Doetschman T, Lorenz JN, Shull GE. Impaired cardiac performance in heterozygous mice with a null mutation in the sarco(endo)plasmic reticulum ca2+-atpase isoform 2 (serca2) gene. *J Biol Chem*. 1999;274:2556-2562
100. Evans-Anderson HJ, Alfieri CM, Yutzey KE. Regulation of cardiomyocyte proliferation and myocardial growth during development by foxo transcription factors. *Circ Res*. 2008;102:686-694
101. Mora A, Davies AM, Bertrand L, Sharif I, Budas GR, Jovanovic S, Mouton V, Kahn CR, Lucocq JM, Gray GA, Jovanovic A, Alessi DR. Deficiency of pdk1 in cardiac muscle results in heart failure and increased sensitivity to hypoxia. *EMBO J*. 2003;22:4666-4676
102. Yano N, Tseng A, Zhao TC, Robbins J, Padbury JF, Tseng YT. Temporally controlled overexpression of cardiac-specific pi3kalpha induces enhanced myocardial contractility--a new transgenic model. *Am J Physiol Heart Circ Physiol*. 2008;295:H1690-1694
103. Guttridge DC. Signaling pathways weigh in on decisions to make or break skeletal muscle. *Curr Opin Clin Nutr Metab Care*. 2004;7:443-450
104. Glass DJ. Signalling pathways that mediate skeletal muscle hypertrophy and atrophy. *Nat Cell Biol*. 2003;5:87-90
105. Glass DJ. Molecular mechanisms modulating muscle mass. *Trends Mol Med*. 2003;9:344-350
106. Glass DJ. Skeletal muscle hypertrophy and atrophy signaling pathways. *Int J Biochem Cell Biol*. 2005;37:1974-1984
107. Bodine SC, Stitt TN, Gonzalez M, Kline WO, Stover GL, Bauerlein R, Zlotchenko E, Scrimgeour A, Lawrence JC, Glass DJ, Yancopoulos GD. Akt/mtor

pathway is a crucial regulator of skeletal muscle hypertrophy and can prevent muscle atrophy in vivo. *Nat Cell Biol*. 2001;3:1014-1019

108. Nader GA, McLoughlin TJ, Esser KA. Mtor function in skeletal muscle hypertrophy: Increased ribosomal rna via cell cycle regulators. *Am J Physiol Cell Physiol*. 2005;289:C1457-1465
109. Pende M. Mtor, akt, s6 kinases and the control of skeletal muscle growth. *Bull Cancer*. 2006;93:E39-43
110. Rommel C, Bodine SC, Clarke BA, Rossman R, Nunez L, Stitt TN, Yancopoulos GD, Glass DJ. Mediation of igf-1-induced skeletal myotube hypertrophy by pi(3)k/akt/mtor and pi(3)k/akt/gsk3 pathways. *Nat Cell Biol*. 2001;3:1009-1013
111. Towler MC, Hardie DG. Amp-activated protein kinase in metabolic control and insulin signaling. *Circ Res*. 2007;100:328-341
112. Vary TC, Lynch CJ. Nutrient signaling components controlling protein synthesis in striated muscle. *J Nutr*. 2007;137:1835-1843
113. Deldicque L, Theisen D, Francaux M. Regulation of mtor by amino acids and resistance exercise in skeletal muscle. *Eur J Appl Physiol*. 2005;94:1-10
114. Wackerhage H, Ratkevicius A. Signal transduction pathways that regulate muscle growth. *Essays Biochem*. 2008;44:99-108
115. Frost RA, Lang CH. Protein kinase b/akt: A nexus of growth factor and cytokine signaling in determining muscle mass. *J Appl Physiol*. 2007;103:378-387
116. Nader GA. Molecular determinants of skeletal muscle mass: Getting the "Akt" Together. *Int J Biochem Cell Biol*. 2005;37:1985-1996
117. Sandri M, Sandri C, Gilbert A, Skurk C, Calabria E, Picard A, Walsh K, Schiaffino S, Lecker SH, Goldberg AL. Foxo transcription factors induce the atrophy-related ubiquitin ligase atrogin-1 and cause skeletal muscle atrophy. *Cell*. 2004;117:399-412
118. Stitt TN, Drujan D, Clarke BA, Panaro F, Timofeyva Y, Kline WO, Gonzalez M, Yancopoulos GD, Glass DJ. The igf-1/pi3k/akt pathway prevents expression of muscle atrophy-induced ubiquitin ligases by inhibiting foxo transcription factors. *Mol Cell*. 2004;14:395-403
119. Luo J, Sobkiw CL, Hirshman MF, Logsdon MN, Li TQ, Goodyear LJ, Cantley LC. Loss of class ia pi3k signaling in muscle leads to impaired muscle growth, insulin response, and hyperlipidemia. *Cell Metab*. 2006;3:355-366
120. Luu YK, Lublinsky S, Ozcivici E, Capilla E, Pessin JE, Rubin CT, Judex S. In vivo quantification of subcutaneous and visceral adiposity by micro-computed tomography in a small animal model. *Med Eng Phys*. 2009;31:34-41

121. Ballou LM, Cross ME, Huang S, McReynolds EM, Zhang BX, Lin RZ. Differential regulation of the phosphatidylinositol 3-kinase/akt and p70 s6 kinase pathways by the alpha(1a)-adrenergic receptor in rat-1 fibroblasts. *J Biol Chem*. 2000;275:4803-4809
122. Morey-Holton ER, Globus RK. Hindlimb unloading rodent model: Technical aspects. *J Appl Physiol*. 2002;92:1367-1377
123. Squire M, Donahue LR, Rubin C, Judex S. Genetic variations that regulate bone morphology in the male mouse skeleton do not define its susceptibility to mechanical unloading. *Bone*. 2004;35:1353-1360
124. Manning BD, Tee AR, Logsdon MN, Blenis J, Cantley LC. Identification of the tuberous sclerosis complex-2 tumor suppressor gene product tuberin as a target of the phosphoinositide 3-kinase/akt pathway. *Mol Cell*. 2002;10:151-162
125. Gupta S, Ramjaun AR, Haiko P, Wang Y, Warne PH, Nicke B, Nye E, Stamp G, Alitalo K, Downward J. Binding of ras to phosphoinositide 3-kinase p110alpha is required for ras-driven tumorigenesis in mice. *Cell*. 2007;129:957-968
126. Zhao JJ, Cheng H, Jia S, Wang L, Gjoerup OV, Mikami A, Roberts TM. The p110alpha isoform of pi3k is essential for proper growth factor signaling and oncogenic transformation. *Proc Natl Acad Sci U S A*. 2006;103:16296-16300
127. Liu Z, Roberts TM. Human tumor mutants in the p110alpha subunit of pi3k. *Cell Cycle*. 2006;5:675-677
128. Deramaudt T, Rustgi AK. Mutant kras in the initiation of pancreatic cancer. *Biochim Biophys Acta*. 2005;1756:97-101
129. Hingorani SR, Petricoin EF, Maitra A, Rajapakse V, King C, Jacobetz MA, Ross S, Conrads TP, Veenstra TD, Hitt BA, Kawaguchi Y, Johann D, Liotta LA, Crawford HC, Putt ME, Jacks T, Wright CV, Hruban RH, Lowy AM, Tuveson DA. Preinvasive and invasive ductal pancreatic cancer and its early detection in the mouse. *Cancer Cell*. 2003;4:437-450
130. Hruban RH, Adsay NV, Albores-Saavedra J, Anver MR, Biankin AV, Boivin GP, Furth EE, Furukawa T, Klein A, Klimstra DS, Kloppel G, Lauwers GY, Longnecker DS, Luttges J, Maitra A, Offerhaus GJ, Perez-Gallego L, Redston M, Tuveson DA. Pathology of genetically engineered mouse models of pancreatic exocrine cancer: Consensus report and recommendations. *Cancer Res*. 2006;66:95-106
131. Crawford HC, Scoggins CR, Washington MK, Matrisian LM, Leach SD. Matrix metalloproteinase-7 is expressed by pancreatic cancer precursors and regulates acinar-to-ductal metaplasia in exocrine pancreas. *J Clin Invest*.

2002;109:1437-1444
132. Yamamoto S, Tomita Y, Hoshida Y, Morooka T, Nagano H, Dono K, Umeshita K, Sakon M, Ishikawa O, Ohigashi H, Nakamori S, Monden M, Aozasa K. Prognostic significance of activated akt expression in pancreatic ductal adenocarcinoma. *Clin Cancer Res*. 2004;10:2846-2850
133. Taniguchi CM, Tran TT, Kondo T, Luo J, Ueki K, Cantley LC, Kahn CR. Phosphoinositide 3-kinase regulatory subunit p85alpha suppresses insulin action via positive regulation of pten. *Proc Natl Acad Sci U S A*. 2006;103:12093-12097
134. Bosco EE, Mulloy JC, Zheng Y. Rac1 gtpase: A "Rac" Of all trades. *Cell Mol Life Sci*. 2009;66:370-374
135. Kimmelman AC, Hezel AF, Aguirre AJ, Zheng H, Paik JH, Ying H, Chu GC, Zhang JX, Sahin E, Yeo G, Ponugoti A, Nabioullin R, Deroo S, Yang S, Wang X, McGrath JP, Protopopova M, Ivanova E, Zhang J, Feng B, Tsao MS, Redston M, Protopopov A, Xiao Y, Futreal PA, Hahn WC, Klimstra DS, Chin L, DePinho RA. Genomic alterations link rho family of gtpases to the highly invasive phenotype of pancreas cancer. *Proc Natl Acad Sci U S A*. 2008;105:19372-19377
136. Qiu RG, Chen J, Kirn D, McCormick F, Symons M. An essential role for rac in ras transformation. *Nature*. 1995;374:457-459
137. Khosravi-Far R, Solski PA, Clark GJ, Kinch MS, Der CJ. Activation of rac1, rhoa, and mitogen-activated protein kinases is required for ras transformation. *Mol Cell Biol*. 1995;15:6443-6453
138. Kallergi G, Agelaki S, Markomanolaki H, Georgoulias V, Stournaras C. Activation of fak/pi3k/rac1 signaling controls actin reorganization and inhibits cell motility in human cancer cells. *Cell Physiol Biochem*. 2007;20:977-986
139. Hubchak SC, Sparks EE, Hayashida T, Schnaper HW. Rac1 promotes tgf-beta-stimulated mesangial cell type i collagen expression through a pi3k/akt-dependent mechanism. *Am J Physiol Renal Physiol*. 2009;297:F1316-1323
140. Tohse N, Seki S, Kobayashi T, Tsutsuura M, Nagashima M, Yamada Y. Development of excitation-contraction coupling in cardiomyocytes. *Jpn J Physiol*. 2004;54:1-6
141. Galindo CL, Skinner MA, Errami M, Olson LD, Watson DA, Li J, McCormick JF, McIver LJ, Kumar NM, Pham TQ, Garner HR. Transcriptional profile of isoproterenol-induced cardiomyopathy and comparison to exercise-induced cardiac hypertrophy and human cardiac failure. *BMC Physiol*. 2009;9:23
142. Vrljicak P, Chang AC, Morozova O, Wederell ED, Niessen K, Marra MA, Karsan

A, Hoodless PA. Genomic analysis distinguishes phases of early development of the mouse atrio-ventricular canal. *Physiol Genomics*. 2010;40:150-157

143. Patino WD, Mian OY, Hwang PM. Serial analysis of gene expression: Technical considerations and applications to cardiovascular biology. *Circ Res*. 2002;91:565-569

144. Bunc M, Suput D, Rozman J. Force transducer for measurement of muscle contraction. *J Med Eng Technol*. 1999;23:222-224

145. McCarthy JJ, Esser KA. Anabolic and catabolic pathways regulating skeletal muscle mass. *Curr Opin Clin Nutr Metab Care*. 2010;13:230-235

146. Masiero E, Agatea L, Mammucari C, Blaauw B, Loro E, Komatsu M, Metzger D, Reggiani C, Schiaffino S, Sandri M. Autophagy is required to maintain muscle mass. *Cell Metab*. 2009;10:507-515